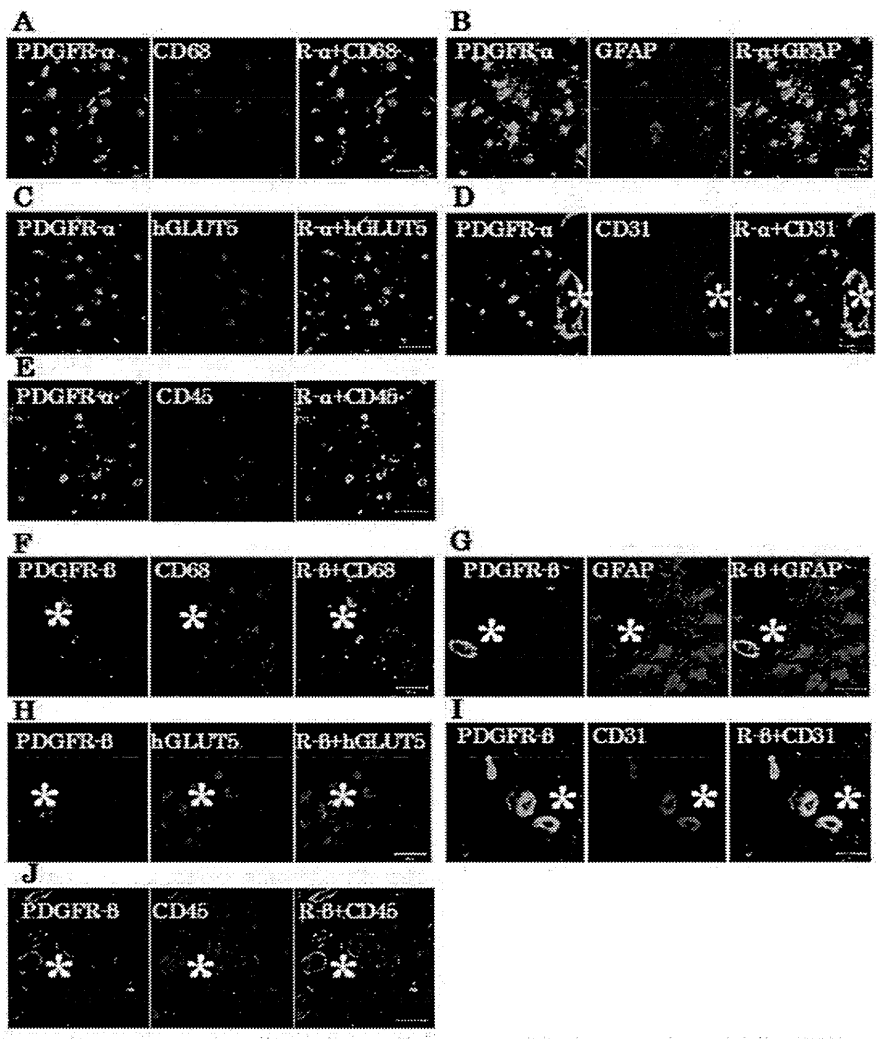

Figure 5 Double immunofluorescence staining. Double immunofluorescence staining from case 1 revealed that PDGFR-α and β were strongly expressed in CD31-positive cells in PN **(D and I)**. PDGFR-α positive cells were merged with many cells positive for CD68 **(A)**, GFAP **(B)**, hGLUT5 **(C)**, and CD45 **(E)**. PDGFR-β-positive cells merged specifically with endothelial cells **(F, G, H, I and J, *)**. Endothelial cells **(*)** were nonspecifically stained with secondary fluorescence antibody. The scale bar represents 50 μm.

angiogenesis and to play a critical role in wound healing [21,27,28].

Li et al. found that PDGF-D is a potent transforming and angiogenic growth factor for NIH/3 T3 cells, and that the transformed cells also induce VEGF expression [28]. Zhao et al. also found that inhibition of PDGF-D leads to decreased cell invasion in gastric cancer, partly through the regulation of VEGF [29]. In our study, many reactive astrocytes produced PDGF-C and D and expressed PDGFR-α, but these cells did not express PDGFR-β. These results established that PDGF-C and D play roles in angiogenesis and inflammation through autocrine and paracrine stimulation. Although the functions of these isoforms of PDGFs on cells are similar in many respects, each isoform might play different roles in different cell types via various receptors and pathways.

Previously, it was reported that several types of cells participate in angiogenesis and inflammation in brain RN [1,5,6]. But the underlying mechanisms have not been completely elucidated. We desperately need to know why different types of cells, including macrophages, microglia, lymphocytes, and astrocytes, acquire the capacity for differentiation, producing inflammatory cytokines and growth factors under certain pathological conditions. Ungvari et al. reported that γ-irradiated cerebromicrovascular endothelial cells acquired a senescence-associated secretory phenotype (SASP) characterized by the upregulation of proinflammatory cytokines and chemokines [30].

Our results suggest that several types of cells that survived irradiation in PN acquired SASP, and that this mechanism may be a key process in brain RN.

In this study, we performed retrospective analysis with clinical specimens of symptomatic RN and revealed that PDGFs/PSGFRs were involved in RN. However, this analysis covers just one aspect of RN. It is impossible to determine whether PDGFs exacerbate RN or rather are produced as a byproduct of RN. Also, we cannot speculate as to the dose–response relationship or the time course of the expression of PDGFs and their receptors in RN. These questions will be answered if a reproducible animal model of RN can be established.

Conclusions

In conclusion, PDGFs/PDGFRs play critical roles in angiogenesis and possibly in inflammation, and they contribute to the pathogenesis of RN, irrespective of the original tumor pathology and applied radiation modality. Moreover, the autocrine or paracrine signaling of PDGFs also plays crucial roles in aggressive angiogenesis and inflammation in RN. PDGF-C, PDGF-D and PDGFR-α have clinical importance, because PDGFR-β was expressed even in UB. Treatments to inhibit PDGF-C and D, or to inhibit PDGF-C and D in combination with PDGFR-α with a kinase inhibitor, may provide new approaches for RN induced by common radiation therapies, including XRT, SRS and BNCT.

Additional files

Additional file 1: Typical MRI of symptomatic radiation necrosis from case 3. Gd-enhanced T1 MRI just prior to excision of necrotic foci (A). Gd-enhanced T1 MRI 2 weeks after surgery (A'). FLAIR MRI just prior to excision of necrotic foci (B). FLAIR MRI, 2 weeks after surgery (B'). After surgical resection of the only enhanced lesion, perilesional edema was decreased compared with preoperative MRI.

Additional file 2: Representative immunohistochemistry from case 1. Immunostaining revealed the necrotic core (A, D NC) and perinecrotic area (A, D PN). PDGF-A (A, B, C) and PDGF-B (D, E) were produced by some monocytic cells (B, E arrow) and endothelial cells (C, E*) in PN. Original magnification, A, D × 40, B, C, E × 200.

Additional file 3: H&E staining and immunohistochemistry from case 3. H&E staining (A) and immunohistochemistry (B through O) from case 3, showing NC and PN. PDGF-A (B, C) and PDGF-B (D, E) were produced by some monocytic cells (arrows in C, E) in PN. In contrast, PDGF-C (F, G, H) and PDGF-D (I, J) were produced by many monocytic cells (arrows in G, H, J), reactive astrocytic cells (arrowheads in G, J), and endothelial cells (H, J*). PDGFR-α (K, L, M) was expressed in monocytic cells (L, arrow), reactive astrocytic cells (L, arrowhead) and endothelial cells (M*) in PN. PDGFR-β (N, O) was expressed mainly in endothelial cells (O*). Original magnification, A, B, D, F, I, K, N × 40, C, E, G, H, J, L, M, O × 200.

Additional file 4: Frequency of expression of PDGFs in the GBM group and non-GBM group. We assessed the frequency of expression of PDGFs semi-quantitatively. In the GBM group (cases 3, 4, 5, 6) and non-GBM group (cases 1, 2, 7), there was no apparent statistical significance in expression of each isoform (A, B, C, D).

Additional file 5: Double immunofluorescence staining results from case 3. Double immunofluorescence staining from case 3 revealed that PDGF-C or D-positive cells were merged with many CD68, hGLUT5, CD45 and GFAP-positive cells. Endothelial cells (*) were nonspecifically stained with secondary fluorescence antibody. The scale bar represents 50 μm.

Additional file 6: Double immunofluorescence staining results from case 3. Double immunofluorescence staining of the specimen from case 3 revealed that PDGFR-α and β were strongly expressed in CD31-positive cells (D and I). PDGFR-α-positive cells were merged with many cells positive for CD68 (A), GFAP (B), hGLUT5 (C), and CD45 (E). PDGFR-β-positive cells were merged specifically with endothelial cells (F thorough J). Endothelial cells (*) were nonspecifically stained with secondary fluorescence antibody. The scale bar represents 50 μm.

Additional file 7: Immunofluorescence staining from consecutive specimens from case 1 and 3. Immunofluorescence staining of consecutive specimens from case 1 (A, B) and 3 (C, D) showed positivity for PDGFR-β (A) or GFAP (B). PDGFR-β (A) was not observable at an excitation wavelength of 561 nm but was apparent at 499 nm in endothelial cells (*). On the other hand, GFAP (B) was observed only at an excitation wavelength of 561 nm in reactive astrocytes. The scale bar represents 50 μm.

Abbreviations

RN: Radiation necrosis; PDGFs: Platelet-derived growth factors; PDGFRs: Platelet-derived growth factor receptors; H&E: Hematoxylin and eosin; PN: Perinecrotic area; UB: Undamaged brain tissue; VEGF: Vascular endothelial growth factor; HIF-1α: Hypoxia-inducible factor 1α; XRT: X-ray treatment; SRS: Stereotactic radiosurgery; Proton: Proton beam therapy; BNCT: Boron neutron capture therapy; NC: Necrotic core; SASP: Senescence-associated secretory phenotype; CTLs: Cytotoxic T-lymphocytes.

Competing interests

The authors declare that they have no competing interests.

Authors' contributions

TM carried out the statistical analysis and drafted the manuscript. S-IM conceived of the study, participated in its design and coordination, and helped to draft the manuscript. TT, NN, MF, HK, EY, SK, and TK participated in the study design and coordination and helped to draft the manuscript. All authors read and approved the final manuscript.

Acknowledgments

This work was partly supported by a Grant-in-Aid for Scientific Research (B) (23390355) and by a Grant-in-Aid for Exploratory Research (24659658) to S-I. M. and by a Grant-in-Aid for Scientific Research (C) (23592145) to M.F. from the Japanese Ministry of Education, Culture, Sports, Science, and Technology. We thank Itsuko Inoue and Kaname Shimokawa for their technical assistance.

Author details

[1]Department of Neurosurgery, Osaka Medical College, 2-7 Daigaku-machi, Takatsuki City, Osaka 569-8686, Japan. [2]Department of Pathology, Osaka Medical College, 2-7 Daigaku-machi, Takatsuki City, Osaka 569-8686, Japan.

Received: 15 October 2013 Accepted: 3 February 2014
Published: 11 February 2014

References

1. Nonoguchi N, Miyatake S, Fukumoto M, Furuse M, Hiramatsu R, Kawabata S, Kuroiwa T, Tsuji M, Ono K: **The distribution of vascular endothelial growth factor-producing cells in clinical radiation necrosis of the brain: pathological consideration of their potential roles.** *J Neurooncol* 2011, 105:423–431.
2. Giglio P, Gilbert MR: **Cerebral radiation necrosis.** *Neurologist* 2003, 9:180–188.
3. Glantz MJ, Burger PC, Friedman AH, Radtke RA, Massey EW, Schold SC Jr: **Treatment of radiation-induced nervous system injury with heparin and warfarin.** *Neurology* 1994, 44:2020–2027.
4. Levin VA, Bidaut L, Hou P, Kumar AJ, Wefel JS, Bekele BN, Grewal J, Prabhu S, Loghin M, Gilbert MR, Jackson EF: **Randomized double-blind placebo-controlled trial of bevacizumab therapy for radiation necrosis of the central nervous system.** *Int J Radiat Oncol Biol Phys* 2011, 79:1487–1495.

5. Furuse M, Nonoguchi N, Kawabata S, Yoritsune E, Takahashi M, Inomata T, Kuroiwa T, Miyatake S: **Bevacizumab treatment for symptomatic radiation necrosis diagnosed by amino acid PET.** *Jpn J Clin Oncol* 2013, **43**:337–341.
6. Miyatake SI, Furuse M, Kawabata S, Maruyama T, Kumabe T, Kuroiwa T, Ono K: **Bevacizumab treatment of symptomatic pseudoprogression after boron neutron capture therapy for recurrent malignant gliomas. Report of 2 cases.** *Neuro-oncology* 2013, 15:650–655.
7. Furuse M, Kawabata S, Kuroiwa T, Miyatake S: **Repeated treatments with bevacizumab for recurrent radiation necrosis in patients with malignant brain tumors: a report of 2 cases.** *J Neurooncol* 2011, **102**:471–475.
8. Arbab AS, Janic B, Jafari-Khouzani K, Iskander AS, Kumar S, Varma NR, Knight RA, Soltanian-Zadeh H, Brown SL, Frank JA: **Differentiation of glioma and radiation injury in rats using in vitro produce magnetically labeled cytotoxic T-cells and MRI.** *PLoS One* 2010, 5:e9365.
9. Kumar S, Arbab AS, Jain R, Kim J, deCarvalho AC, Shankar A, Mikkelsen T, Brown SL: **Development of a novel animal model to differentiate radiation necrosis from tumor recurrence.** *J Neurooncol* 2012, **108**:411–420.
10. Heldin CH, Westermark B: **Mechanism of action and in vivo role of platelet-derived growth factor.** *Physiol Rev* 1999, **79**:1283–1316.
11. Heldin CH, Ostman A, Ronnstrand L: **Signal transduction via platelet-derived growth factor receptors.** *Biochim Biophys Acta* 1998, **1378**:F79–F113.
12. Bergsten E, Uutela M, Li X, Pietras K, Ostman A, Heldin CH, Alitalo K, Eriksson U: **PDGF-D is a specific, protease-activated ligand for the PDGF beta-receptor.** *Nat Cell Biol* 2001, 3:512–516.
13. Li X, Ponten A, Aase K, Karlsson L, Abramsson A, Uutela M, Backstrom G, Hellstrom M, Bostrom H, Li H, *et al*: **PDGF-C is a new protease-activated ligand for the PDGF alpha-receptor.** *Nat Cell Biol* 2000, 2:302–309.
14. Wang Z, Ahmad A, Li Y, Kong D, Azmi AS, Banerjee S, Sarkar FH: **Emerging roles of PDGF-D signaling pathway in tumor development and progression.** *Biochim Biophys Acta* 1806, **2010**:122–130.
15. Lei H, Kazlauskas A: **Focus on molecules: platelet-derived growth factor C, PDGF-C.** *Exp Eye Res* 2008, **86**:711–712.
16. Wang Z, Kong D, Banerjee S, Li Y, Adsay NV, Abbruzzese J, Sarkar FH: **Down-regulation of platelet-derived growth factor-D inhibits cell growth and angiogenesis through inactivation of Notch-1 and nuclear factor-kappaB signaling.** *Cancer Res* 2007, **67**:11377–11385.
17. Hoch RV, Soriano P: **Roles of PDGF in animal development.** *Development* 2003, **130**:4769–4784.
18. Li R, Maminishkis A, Wang FE, Miller SS: **PDGF-C and -D induced proliferation/migration of human RPE is abolished by inflammatory cytokines.** *Invest Ophthalmol Vis Sci* 2007, **48**:5722–5732.
19. Lindahl P, Johansson BR, Leveen P, Betsholtz C: **Pericyte loss and microaneurysm formation in PDGF-B-deficient mice.** *Science* 1997, **277**:242–245.
20. Li X, Kumar A, Zhang F, Lee C, Li Y, Tang Z, Arjuna P: **VEGF-independent angiogenic pathways induced by PDGF-C.** *Oncotarget* 2010, 1:309–314.
21. Uutela M, Wirzenius M, Paavonen K, Rajantie I, He Y, Karpanen T, Lohela M, Wiig H, Salven P, Pajusola K, *et al*: **PDGF-D induces macrophage recruitment, increased interstitial pressure, and blood vessel maturation during angiogenesis.** *Blood* 2004, **104**:3198–3204.
22. Deuel TF, Senior RM, Huang JS, Griffin GL: **Chemotaxis of monocytes and neutrophils to platelet-derived growth factor.** *J Clin Invest* 1982, **69**:1046–1049.
23. Kumagai S, Ohtani H, Nagai T, Funa K, Hiwatashi N, Shimosegawa T, Nagura h: **Platelet-derived growth factor and its receptors are expressed in areas of both active inflammation and active fibrosis in inflammatory bowel disease.** *Tohoku J Exp Med* 2001, 195:21–33.
24. Leibovich SJ, Ross R: **The role of the macrophage in wound repair. A study with hydrocortisone and antimacrophage serum.** *Am J Pathol* 1975, **78**:71–100.
25. Gilbertson DG, Duff ME, West JW, Kelly JD, Sheppard PO, Hofstrand PD, Gao Z, Shoemaker K, Bukowski TR, Moore M, *et al*: **Platelet-derived growth factor C (PDGF-C), a novel growth factor that binds to PDGF alpha and beta receptor.** *J Biol Chem* 2001, **276**:27406–27414.
26. Cao R, Brakenhielm E, Li X, Pietras K, Widenfalk J, Ostman A, Eriksson U, Cao Y: **Angiogenesis stimulated by PDGF-CC, a novel member in the PDGF family, involves activation of PDGFR-alphaalpha and -alphabeta receptors.** *FASEB J* 2002, 16:1575–1583.
27. LaRochelle WJ, Jeffers M, Corvalan JR, Jia XC, Feng X, Vanegas S, Vickroy JD, Yang XD, Chen F, Gazit G, *et al*: **Platelet-derived growth factor D: tumorigenicity in mice and dysregulated expression in human cancer.** *Cancer Res* 2002, **62**:2468–2473.
28. Li H, Fredriksson L, Li X, Eriksson U: **PDGF-D is a potent transforming and angiogenic growth factor.** *Oncogene* 2003, **22**:1501–1510.
29. Zhao L, Zhang C, Liao G, Long J: **RNAi-mediated inhibition of PDGF-D leads to decreased cell growth, invasion and angiogenesis in the SGC-7901 gastric cancer xenograft model.** *Cancer Biol Ther* 2010, 9:42–48.
30. Ungvari Z, Podlutsky A, Sosnowska D, Tucsek Z, Toth P, Deak F, Gautam T, Csiszar A, Sonntag WE: **Ionizing radiation promotes the acquisition of a senescence-associated secretory phenotype and impairs angiogenic capacity in cerebromicrovascular endothelial cells: role of increased DNA damage and decreased DNA repair capacity in microvascular radiosensitivity.** *J Gerontol Series A, Biol Sci Med Sci* 2013, **68**:1443–1457.

doi:10.1186/1748-717X-9-51
Cite this article as: Miyata *et al.*: The roles of platelet-derived growth factors and their receptors in brain radiation necrosis. *Radiation Oncology* 2014 **9**:51.

J Neurosurg 120:1–11, 2014

Surgical outcomes of the minimum anterior and posterior combined transpetrosal approach for resection of retrochiasmatic craniopharyngiomas with complicated conditions

Clinical article

Noritsugu Kunihiro, M.D., Takeo Goto, M.D., Kenichi Ishibashi, M.D., and Kenji Ohata, M.D.

Department of Neurosurgery, Osaka City University Graduate School of Medicine, Osaka, Japan

Object. Retrochiasmatic craniopharyngiomas are surgically challenging tumors. Retrochiasmatic craniopharyngiomas with complicated conditions such as large diameter, major calcification, or significant extension to the third ventricle or posterior fossa present surgical challenges; moreover, recurrent retrochiasmatic craniopharyngiomas are particularly formidable challenges. Although the transpetrosal approach to retrochiasmatic craniopharyngiomas published by Hakuba in 1985 can provide unique advantageous exposure of the retrochiasmatic area to allow safe neurovascular dissection and facilitate radical tumor removal, the procedure is viewed as complicated and time consuming and has a high risk of damaging hearing functions. The authors have modified Hakuba's technique to minimize petrosectomy and reduce surgical complications and have applied this modified approach to retrochiasmatic craniopharyngiomas with complicated conditions. In this study, the authors describe their technique and surgical outcomes to elucidate the role of this modified transpetrosal approach for retrochiasmatic craniopharyngiomas with complicated conditions. This is the first study to report surgical outcomes of the transpetrosal approach for retrochiasmatic craniopharyngiomas.

Methods. Between 1999 and 2011, the minimum anterior and posterior combined (MAPC) transpetrosal approach, which is a modification of Hakuba's transpetrosal approach, was applied in 16 cases of retrochiasmatic craniopharyngiomas with complicated conditions. Eight cases were recurrent tumors, 4 had previously received radiotherapy, 11 had a large diameter, 10 had large calcification, 15 had superior extension of the tumor into the third ventricle, and 10 had a posterior extension of the tumor that compressed the midbrain and pons. In all 16 patients, more than 2 of these complicated conditions were present. The follow-up duration ranged from 0.8 to 12.5 years (mean 5.3 years). Surgical outcomes assessed were the extent of resection, surgical complications, visual function, endocrinological status, and neuropsychological function. Five-year and 10-year recurrence-free survival rates were also calculated.

Results. Gross-total or near-total resection was achieved in 15 cases (93.8%). Facial nerve function was completely maintained in all 16 patients. Serviceable hearing was preserved in 15 cases (93.8%). Visual function improved in 13 out of 14 cases (92.9%) that had visual disturbance before surgery. None of the patients experienced deterioration of their visual function. Twelve cases had endocrinological deficit and received hormonal replacement before surgery. New endocrinological deficit occurred in 2 cases (12.5%). Neuropsychological function was maintained in 14 cases (87.5%) and improved in 1 case (6.3%). One case that had received previous conventional radiotherapy treatment showed a gradual decline in neuropsychological function. The 5-year and 10-year recurrence-free survival rates were both 86.5%.

Conclusions. The authors obtained good results by using the MAPC transpetrosal approach for the removal of retrochiasmatic craniopharyngiomas with complicated conditions. The MAPC transpetrosal approach should be considered as a therapeutic option for selected cases of retrochiasmatic craniopharyngiomas with complicated conditions.

(http://thejns.org/doi/abs/10.3171/2013.10.JNS13673)

Key Words • **retrochiasmatic craniopharyngioma** • **skull base** • **surgical approach** • **transpetrosal approach** • **oncology**

Craniopharyngiomas located in retrochiasmatic regions are regarded as particularly challenging tumors to remove safely and totally because of their anatomical location and proximity to critical neurovascular structures.[2,6,26] Surgical resection of this type of craniopharyngioma is associated with high rates of surgical mortality, surgical complications, and incomplete resection resulting in a high recurrence rate.[6,26] Although various surgical approaches to remove retrochiasmatic craniopharyngiomas have been described, including pterional, orbitopterional, orbitozygomatic, transbasal subfrontal, frontobasal interhemispheric, and transnasal transsphenoi-

Abbreviations used in this paper: KPS = Karnofsky Performance Scale; MAPC = minimum anterior and posterior combined; PCoA = posterior communicating artery; VIS = visual impairment scale

dal approaches,[3,5,6,8,10,15–17,22,23,26,29] the optimal surgical approach remains controversial.

In 1985, Hakuba reported the usefulness of the transpetrosal approach for the removal of retrochiasmatic craniopharyngiomas,[11] emphasizing that this approach offers wide exposure of retrochiasmatic lesions and unique posterior-to-anterior and inferior-to-superior projection to the inferior and posterior surfaces of the chiasm, the floor of third ventricle, and the hypothalamic tuber cerium area. However, in his approach, Hakuba sacrificed 3 semicircular canals with 33% hearing preservation. Al-Mefty et al. used Hakuba's techniques and reported the effectiveness of the transpetrosal approach for giant retrochiasmatic craniopharyngiomas[1] but have not yet reported outcomes and complication rates in their surgical series. In addition, the complicated surgical procedures involved in the petrosal approach have discouraged neurosurgeons from assessing the most effective approach for removal of retrochiasmatic craniopharyngiomas.

We have modified Hakuba's techniques to minimize petrosectomy and reduce surgical complications and have applied this approach to 16 patients with retrochiasmatic craniopharyngiomas with complicated conditions such as a history of excision or radiotherapy, tumors with large calcification, large diameter (> 30 mm), superior extension into the third ventricle, or severe posterior extension compressing the midbrain and pons. This study retrospectively analyzed surgical outcomes, including the extent of tumor resection, recurrence rate, surgical complications, visual function, endocrinological status, neuropsychological function, and functional performance status, to elucidate the role of our modified transpetrosal approach for the removal of retrochiasmatic craniopharyngioma with complicated conditions. This is the first study to report surgical outcomes of the transpetrosal approach for retrochiasmatic craniopharyngioma.

Methods

Indications for MAPC Transpetrosal Approach

Minimum anterior and posterior combined (MAPC) transpetrosal approaches were applied to retrochiasmatic craniopharyngiomas with complicated conditions such as a history of excisions or radiotherapy, tumors with large calcification, large diameter (> 30 mm), superior extension into the third ventricle, or severe posterior extension compressing the midbrain and pons. If a retrochiasmatic craniopharyngioma possessed not less than 2 of these complicated conditions and no well-developed middle fossa venous sinus (such as the sphenobasal or sphenopetrosal sinus) blocking the surgical route to the tumor, the MAPC transpetrosal approach was applied.

Patient Population

Between 1999 and 2011, a total of 44 consecutive patients underwent resection of craniopharyngiomas in the Department of Neurosurgery at Osaka City University in Osaka, Japan. Medical records from all 44 patients were retrospectively examined. Tumors showing the following conditions on imaging were defined as retrochiasmatic craniopharyngiomas: 1) the tumor extending toward the posterior fossa and upward toward the third ventricle, displacing the midbrain posteriorly and the optic chiasm anteriorly; and 2) no upward displacement of the anterior cerebral arteries as would be seen in patients with a prechiasmatic craniopharyngioma. Thirty-six of the 44 tumors were classified as retrochiasmatic craniopharyngioma and 16 of these 36 tumors were resected using our modified MAPC transpetrosal approach. These 16 cases formed the sample for this study. All clinical data of the 16 patients were reviewed retrospectively.

Six patients were male and 10 patients were female, and their mean age at the time of surgery was 47.9 years (range 27–71 years; Table 1). Eight patients (50.0%) had undergone previous surgical procedures at other institutions (Table 1). Prior surgical approaches were interhemispheric in 3 patients, pterional in 2, extended transsphenoidal in 2, and orbitozygomatic in 2. Ommaya reservoirs had been placed in 2 patients. Four patients had received repeated or combined operations. The mean interval between first surgery and our surgery was 10.0 years (range 0.7–32.0 years). Four patients had already received radiotherapy prior to referral to our institution. Stereotactic radiosurgery was added in 2 cases, conventional radiotherapy to 1, and conventional radiotherapy and 3 sessions of stereotactic radiosurgery in 1. The mean maximum diameter of the tumor, as estimated from preoperative MR images, was 32.1 mm (range 25–40 mm). A large tumor diameter (maximum tumor diameter > 30 mm) was present in 11 patients (68.8%). A large calcification (intratumoral calcification > 10% of tumor volume on preoperative CT images) was present in 10 patients (62.5%). Superior extension into the third ventricle was documented in 15 patients (93.8%). Posterior extension in which the tumor appeared to be compressing the midbrain and pons was present in 10 patients (62.5%). All 16 patients had no fewer than 2 of these complicated conditions (Table 1).

Nine tumors were removed in a single step via the MAPC transpetrosal approach and 7 tumors were excised in 2 steps via a combination of the MAPC transpetrosal approach and other approaches (for example, orbitozygomatic, interhemispheric lamina terminalis, and transsphenoidal). The mean follow-up duration was 5.3 years (range 0.8–12.5 years). The median survival duration was 5.6 years (range 1.4–12.5 years). Three patients died during the follow-up period: 1 patient of radiation necrosis 3.6 years after surgery; 1 of chronic heart failure 6.1 years after surgery; and 1 of old age 1.7 years after surgery. Another patient was followed up for 0.8 years before being lost to follow-up after being transferred to another hospital for an unrelated disease 1.4 years after surgery. Clinical and ophthalmological examinations, imaging studies, endocrinological studies, neuropsychological function, and surgical complications were reviewed retrospectively based on the medical records at our institution.

Neuroradiological Evaluation

Before surgery, all patients underwent MRI, CT, and angiography. Tumor size was estimated from MR images by measuring the maximum anteroposterior, vertical, and horizontal diameters. The extent of intratumoral calcifica-

TABLE 1: Characteristics of 16 patients with tumors resected via the MAPC transpetrosal approach*

Case No.	Age (yrs), Sex	Previous Op	Interval Btwn Ops (yrs)†	Previous Radiation	Max Tumor Diameter (mm)	Calcification (%)	Superior Extension into 3rd Ventricle	Posterior Extension Compressing Brainstem
1	31, F				25	>50	yes	no
2	63, F	PT × 4	32	conventional RT	32	<10	yes	yes
3	69, F				40	>10	yes	yes
4	27, F	OZ × 2, Ommaya	1.6		27	>10	yes	yes
5	60, F				30	none	yes	no
6	30, M				31	none	yes	no
7	39, M	IH	3.7	SRS	36	none	yes	yes
8	71, F				37	>50	yes	no
9	69, M				36	none	yes	yes
10	45, M				31	<10	yes	yes
11	34, F	OZ, extended TSS	1.2		25	>10	no	no
12	47, M	extended TSS	0.7		38	>10	yes	yes
13	69, F				30	>50	yes	yes
14	33, F	PT × 3, Ommaya × 2	18	SRS × 3, conventional RT	25	>50	yes	no
15	33, M	IH	5.3	SRS	26	>50	yes	yes
16	61, F	IH	18		44	>10	yes	yes

* IH = interhemispheric approach; OZ = orbitozygomatic approach; PT = pterional approach; RT = radiation therapy; SRS = stereotactic radiosurgery; TSS = transsphenoidal surgery.

† Interval between first surgery and surgery at our institution.

tion was determined on CT images. Intratumoral calcification that accounted for more than 10% of the tumor volume was defined as large calcification. Anatomical features of the cerebral vessels, such as the extent of development of the posterior communicating artery (PCoA) and the development of venous drainage on the lesion side, were evaluated on angiograms. Precise understanding of venous flow in the middle and posterior fossa is mandatory to safely complete the transpetrosal approach. For example, the insertion of the petrosal vein into the superior petrosal sinus represents a key landmark for ligation of the superior petrosal sinus and the cerebellar tentorium. In addition, a well-developed sphenobasal sinus without sufficient collateral venous flow represents one of the most significant hazards to the transpetrosal approach. These fine venous findings can currently only be obtained on 3D angiography. We therefore performed angiography in all cases in addition to MR angiography.

Extent of Tumor Resection

Neuroradiologists independently reviewed the results of preoperative and postoperative MR and CT images to assess the extent of tumor resection. The extent of resection was determined from MR and CT images obtained within 1 week after surgery and from follow-up radiological studies. All tumors were evaluated using enhanced MRI. However, small calcifications can only be detected on CT, which is why this modality was used for radiological evaluation. If small calcifications were identified, a small residual tumor was considered to be present. Small enhanced lesions that diminished in the late period were judged as representing postoperative reactive changes rather than as residual tumor.

Resection was classified as gross-total resection when there was no residual enhanced lesion or residual calcification, near-total resection when residual enhanced lesion or calcification was limited to less than 0.5 cm^3, and subtotal resection when there was residual enhanced lesion or calcification was equal to or less than 0.5 cm^3. The volume of the residual enhanced lesion or calcification was calculated as the volume of an ellipsoid: volume = $4\pi abc/3 \times 2^3$, where a, b, and c represent the orthogonal diameters on the MR image.

Tumor Recurrence

Follow-up MRI was performed within 1 week after surgery, within 3 months after surgery, and then at regular intervals of 6–12 months. Three patients underwent the second MRI session at 4 months after surgery rather than within 3 months. All other patients underwent MRI in accordance with the schedule. Recurrence of the tumor during follow-up was defined as the appearance of new pathological tissue on MR images or the growth of tumor remnants.

Visual Function

Ophthalmological evaluation, including visual acuity and field examination in accordance with the guidelines of the German Ophthalmological Society, was performed by an ophthalmologist before and after surgery and when clinically appropriate. The timing of subsequent assess-

ments was decided on an individual basis. Visual function was quantified using the visual impairment scale (VIS), which is based on visual acuity and visual field defects in both eyes (Fig. 1).[7] Available ophthalmological examinations including visual acuity and visual field testing for reviews were performed in 15 cases. One patient who was transferred to another hospital for an unrelated disease during the follow-up period did not undergo full ophthalmological evaluation.

Endocrinological Status

In addition to clinical symptoms, we evaluated basic levels of luteinizing hormone, follicle-stimulating hormone, free triiodothyronine, free thyroxine, thyroid-stimulating hormone, growth hormone, cortisol, adrenocorticotropic hormone, and prolactin before and after surgery. Anterior pituitary hormone dysfunction was defined as the use of hormone supplementation; deficits in basic levels of luteinizing hormone, follicle-stimulating hormone, free triiodothyronine, free thyroxine, thyroid-stimulating hormone, growth hormone, cortisol, or adrenocorticotropic hormone; or high levels of prolactin without use of dopamine agonists. Diabetes insipidus was diagnosed before and after surgery based on sodium level and the presence of hypotonic polyuria. All patients underwent available endocrinological assessment for review.

Neuropsychological Function

Neuropsychological function was evaluated preoperatively and postoperatively by face-to-face examinations. Patients were classified as showing neuropsychological dysfunction if any of the following conditions were met: 1) score < 70 on the full scale of the Wechsler adult intelligence scale (3rd edition);[28] 2) score < 20 on the Mini-Mental Status Examination;[9] or 3) the patient found it impossible to continue in a previous occupation. These data were available for review from all patients.

Functional Performance Status

Functional performance status was evaluated using the Karnofsky Performance Scale (KPS).

Statistical Analysis

The cumulative risk of tumor recurrence was calculated according to the Kaplan-Meier method; JMP 9.0 software (SAS Institute Inc.) was used.

The MAPC Transpetrosal Approach

Positioning. Patients were placed in a semiprone park bench position. The head was fixed using 3-point fixation with the head rotated and vertex down to keep the temporal side of the head in the horizontal plane.

Skin Incision. The skin incision started at the upper margin of the zygomatic arch anterior to the tragus, turned 2–3 cm above the ear, and then descended behind the posterior margin of the mastoid process. After reflecting the skin flap, a temporal fascia-pericranial flap with a pedicle of the sternocleidomastoid muscle was harvested to prevent leakage of CSF.

Craniotomy. Temporo-occipito-suboccipital craniotomy was performed prior to mastoidectomy. Key bur holes were placed at 4 anatomical landmarks to avoid injuring the sigmoid sinus. The first bur hole was made at the asterion, the second at the intersection of the supramastoid crest with the squamous suture, the third at the mastoid emissary foramen, and the fourth just at the inion-asterion line. The first bur hole was usually just above the lateral end of the transverse sinus, the second just anterior to the transverse-sigmoid sinus junction, the third a few millimeters medial to the posterior edge of the sigmoid sinus, and the fourth just on the transverse sinus.

Preparation for MAPC Petrosectomy. After temporo-occipito-suboccipital craniotomy, the outer cortical bone of the mastoid portion of the temporal bone was removed as a thin triangular plate for cosmetic mastoidectomy. This procedure was not essential and was skipped in cases in which the groove of the sigmoid sinus was too large. At this point, the transverse sinus and transverse sinus–sigmoid sinus junction had been safely exposed (Fig. 2A). Dural dissection from the petrous and mastoid portions of the temporal bone was then started for safe and swift petrosectomy. At the middle fossa, the dura matter at the temporal base was gently reflected to fully expose the entire course of the petrous ridge and apex by cutting the middle meningeal artery and dissecting the greater superficial petrosal nerve. At the posterior fossa, the presigmoid dura was carefully dissected from the posterior surface of the petrous portion of the temporal bone and the entrance of the internal auditory canal was epidurally exposed by cutting the endolymphatic sac (Fig. 2B). After completion of this dural dissection, bone work for petrosectomy was performed (Fig. 2C). This full dural retraction is a unique characteristic of the MAPC transpetrosal approach. The membranous labyrinths of the semicircular canals were kept intact to preserve hearing. A small amount of bone at the petrous ridge was drilled out to obtain a surgical corridor along the axis of the petrous ridge (Fig. 2D and E). The amount of petrous portion of the temporal bone required for petrosectomy is quite limited and this allows a quick surgical procedure.

Dural Opening. The presigmoid dura was opened along the drilled petrosal portion of the temporal bone as far anteriorly as possible while the insertion of the petrosal vein at the superior petrosal sinus was inspected. The subtemporal dura was opened anteriorly and the superior petrosal sinus was divided by Weck clips (Teleflex) at a point anterior to the insertion of the petrosal vein at the superior petrosal sinus to preserve venous reflux from the petrosal vein. The tentorium was cut behind the dural entrance of the trochlear nerve, and the trochlear nerve into the tentorium was exposed.

Intradural Procedure. After superior retraction of the temporal lobe and medial mobilization of the sigmoid sinus, the arachnoid membrane was dissected to obtain a surgical corridor to the retrochiasmatic space (Fig. 3A). The trochlear nerve, oculomotor nerve, C_1 and C_2 portions of the internal carotid artery, PCoA and its perforating branches, posterior cerebral artery, and superior cerebellar artery were identified step by step; the tumor was widely

Visual acuity

R \ L	1,0	0,8	0,63	0,5	0,4	0,32	0,25	0,2	0,16	0,1	0,08	0,05	0,02	0
	5/5	5/8	5/8	5/10	5/12	5/15	5/20	5/25	5/30	5/50	1/12	1/20	1/50	0
1,00	5/5	0	2	4	6	8	10	12	15	17	20	22	25	27	30
0,8	5/8	2	4	8	10	12	15	17	20	22	25	27	30	32	35
0,63	5/8	4	8	15	17	20	22	25	27	30	32	35	37	40	42
0,5	5/10	6	10	17	20	22	25	27	30	32	35	40	42	45	47
0,4	5/12	8	12	20	22	25	30	32	35	37	40	42	47	50	52
0,32	5/15	10	15	22	25	30	35	40	45	47	50	55	57	60	62
0,25	5/20	12	17	25	27	32	40	50	52	55	57	60	65	67	70
0,2	5/25	15	20	27	30	35	45	52	55	57	60	65	70	75	80
0,16	5/30	17	22	30	32	37	47	55	57	60	65	70	75	80	85
0,1	5/50	20	25	32	35	40	50	57	60	65	75	80	85	87	90
0,08	1/12	22	27	35	40	42	55	60	65	70	80	85	90	92	95
0,05	1/20	25	30	37	42	47	57	65	70	75	85	90	95	100	100
0,02	1/50	28	32	40	45	50	60	67	75	80	87	92	100	100	100
0	0	30	35	42	47	52	62	70	80	85	90	95	100	100	100

Visual field defect

R \ L											
	0	2	4	5	5	5	5	5	5	5	0
	2	6	8	8	10	14	18	19	20	25	2
	4	8	10	12	14	16	20	21	22	27	4
	5	8	12	14	16	18	22	22	23	28	6
	5	10	14	16	18	20	22	23	24	29	8
	5	14	16	18	20	22	24	25	26	31	10
	5	18	20	22	22	24	26	28	35	40	15
	5	19	21	22	23	25	28	30	40	45	20
	5	20	22	23	24	26	35	40	45	48	25
	5	25	27	28	29	31	40	45	48	50	25
	0	2	4	6	8	10	15	20	25	25	0

Fig. 1. Tables of visual acuity and visual field defects used to calculate the VIS score. The *black boxes with numbers* provide an example of the calculation made in a patient with a visual acuity of 0.4 in the left eye and 0.2 in the right eye, together with a bitemporal visual field defect. The VIS score is the sum of these 2 numbers (that is, 35 + 22 = 57). Reprinted with permission from Fahlbusch R, Schott W: *J Neurosurg 96*:235–243, 2002.

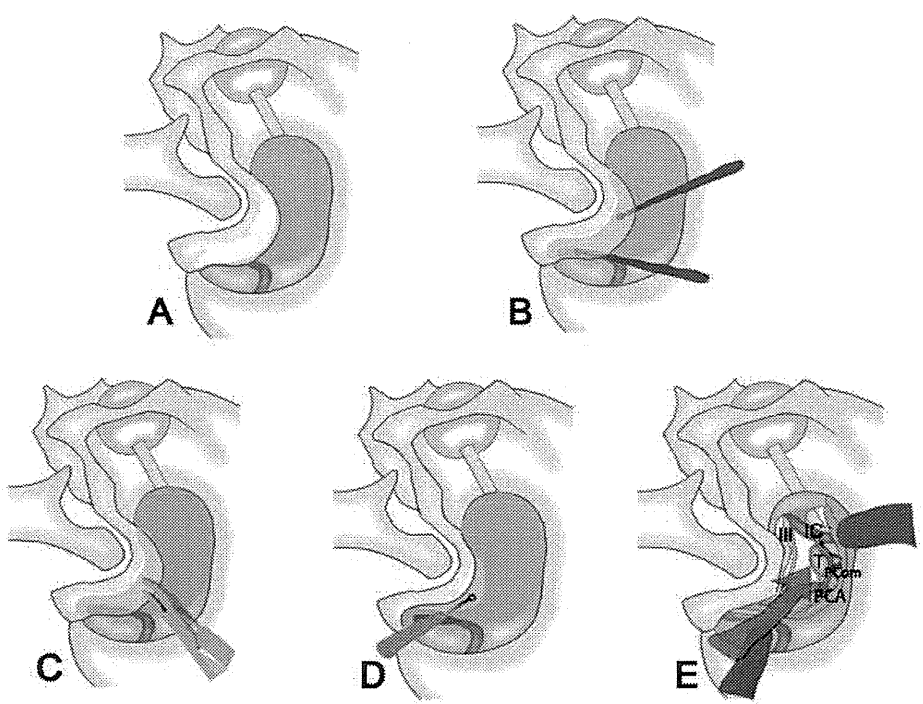

Fig. 2. Illustrations of petrosectomy used in the MAPC transpetrosal approach. **A:** The transverse sinus and transverse sinus–sigmoid sinus junction are safely exposed after temporo-occipito-suboccipital craniotomy and cosmetic mastoidectomy. **B:** Dural dissection from the petrous and mastoid portions of the temporal bone is completely performed at the middle fossa and the posterior fossa. **C:** Complete exposed petrous portion of temporal bone is safely and quickly removed in the wide surgical field. **D:** A small amount of bone at the petrous ridge is drilled out to create a unique surgical corridor. **E:** The wide exposure and unique posterior-to-anterior and inferior-to-superior projection for retrochiasmatic craniopharyngiomas are offered by the MAPC transpetrosal approach *(red arrow)*. IC = internal carotid artery; PCA = posterior cerebral artery; PCom = PCoA; T = tumor; III = third cranial nerve. Copyright Noritsugu Kunihiro. Published with permission.

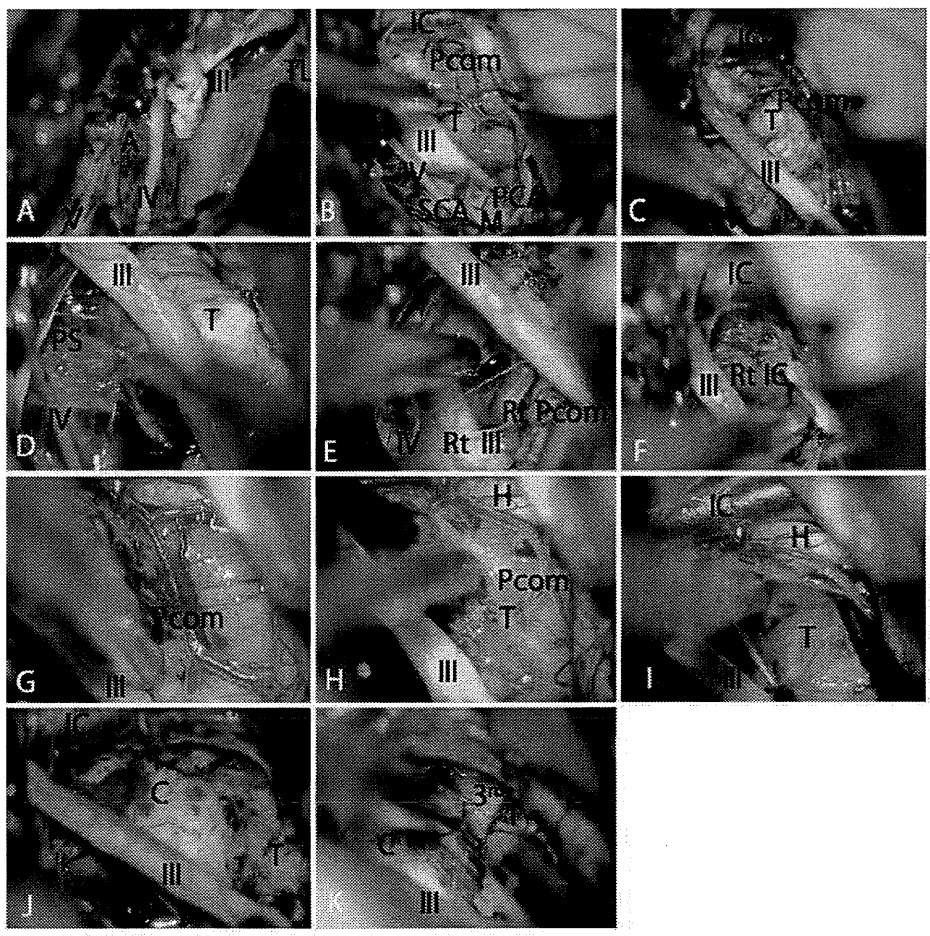

Fig. 3. Intraoperative photographs of intradural exposure and tumor removal achieved using the MAPC transpetrosal approach. **A:** Initial exposure of the vital retrochiasmatic space reveals cranial nerves covered with arachnoid membrane (A). **B:** The corridor of the MAPC transpetrosal approach is widely exposed to reveal the tumor (T) and vital neurovascular structures near the tumor. **C:** The space between the oculomotor nerve (III) and PCoA (Pcom) as well as below the oculomotor nerve provides wide surgical fields for tumor resection. **D:** The pituitary stalk (PS) is well visualized through the space below the oculomotor nerve. **E and F:** The right oculomotor nerve (Rt III), the right PCoA (Rt Pcom), and the right internal carotid artery (Rt IC) are well visualized. This allows preservation of perforating arteries from the PCoA. **G and H:** The upward mobilization that follows the division of the PCoA; the mobilization offers wider operative space and wide exposure of the tumor around the inferior surface of the hypothalamus (H). **I:** The direct visualization of the change in appearance of tissue between the tumor and hypothalamus provides a safe gliotic plane of dissection. **J:** The inferior and posterior surface of the chiasm (C) is well visualized via posterior-to-anterior and inferior upward projection. **K:** The medial wall of the third ventricle (3rd) is well visualized after more upward projection. IV = fourth cranial nerve; M = midbrain; PCA = posterior cerebral artery; SCA = superior cerebellar artery; TL = temporal lobe; V = fifth cranial nerve.

exposed behind the optic chiasm, under the hypothalamus, and in front of the midbrain (Fig. 3B). In this approach, the space between the oculomotor nerve and PCoA, as well as below the oculomotor nerve, provided useful surgical fields for tumor resection. After the initial internal decompression of the tumor (Fig. 3C), the pituitary stalk was visualized (Fig. 3D) but not often preserved. The inferior portion of the tumor on the contralateral side was dissected from the contralateral oculomotor nerve, PCoA, and internal carotid artery (Fig. 3E and F). The main corridor between the oculomotor nerve and PCoA allowed safe dissection from the surrounding structures, such as the surface behind the chiasm or hypothalamus on direct visualization. The hypoplastic PCoA was often divided at the intersection point with the posterior cerebral artery, and upward mobilization of the PCoA enlarged the operative space (Fig. 3G and H). By obtaining more upward projection through this wider operative space, the tumor was safely dissected off the inferior surface of the hypothalamus (Fig. 3I). As dissection progressed anteriorly, the inferior and posterior surfaces of the chiasm were visualized directly via posterior-to-anterior and inferior-to-superior projection (Fig. 3J). In cases where the tumor extended into posterior fossa, it was dissected away from the basilar artery or lower cranial nerves. The intraventricular part of the tumor with superior extension was dissected from the medial wall of the third ventricle under direct visualization through the more upward projection (Fig. 3K).

Closure. All opened mastoid air cells were sealed with abdominal fat-soaked fibrin glue; then the mastoid and petrous portions of the temporal bone and dural defect were entirely covered with the harvested fascia-pericranial flap. The lumbar drain was left open for approximately 3 days to allow CSF pressure to reduce and prevent leakage of CSF.

Results

Extent of Tumor Resection

The extent of tumor resection is shown in Table 2. Gross-total resection was achieved in 9 patients (56.3%) and near-total resection was achieved in 6 patients (37.5%). Subtotal resection was found in only 1 patient (Case 2). This patient had particularly complicated conditions, including 4 previous surgeries and a history of conventional radiation therapy.

Tumor Recurrence

During the follow-up period, no tumor recurrence occurred in any of the 9 patients with gross-total resection (Table 2). Regrowth was detected in 1 of the 6 patients with near-total resection but was successfully controlled for 108 months after an additional resection and stereotactic radiosurgery. Regrowth began 8 months after surgery in the patient with subtotal resection. This was controlled by additional resection and stereotactic radiosurgery treatment, but the patient died due to radiation necrosis.

Morbidity and Mortality

No surgery-related deaths occurred. Transient oculomotor nerve palsy was confirmed in 7 patients and was fully resolved within the follow-up period. Facial nerve function was completely maintained in all 16 patients. Serviceable hearing was preserved in 15 of the 16 patients. No other cranial nerve palsies were seen. Venous infarction or contusion-related temporal retraction was not detected. Leakage of CSF and surgical-site infection did not occur in any patients (Table 2).

Visual Function

Results of the VIS are presented in Table 2. Fifteen patients (93.8%) showed visual disturbance before surgery. One patient who was lost to follow-up after admission to another hospital with an unrelated disease did not undergo a full ophthalmological evaluation and thus was not included in this analysis. One patient with normal visual function preoperatively retained normal function postoperatively. Visual function improved after surgery in 13 (92.9%) of the 14 patients who had visual disturbance before surgery. One patient (Case 2) did not show improvement in visual function after surgery. This patient was blind in both eyes (VIS score of 100) before surgery. No patients experienced any deterioration in visual function. The mean VIS score improved from 37.2 ± 33.7 preoperatively to 17.3 ± 31.3 postoperatively.

Endocrinological Status

Twelve patients (75.0%) had an endocrinological deficit or had received hormonal replacement before our surgery. Preoperatively, 4 patients had received replacement of anterior pituitary hormone, 6 patients showed a deficit in anterior pituitary hormone, and 9 patients had diabetes insipidus. Three patients showed deficit of anterior pituitary hormone without diabetes insipidus and 2 patients showed only diabetes insipidus. Postoperatively, 14 patients (87.5%) received endocrine replacement (Table 2). Of these patients, 2 received replacement of anterior pituitary hormone without diabetes insipidus and 1 had diabetes insipidus only. Pituitary stalks were anatomically preserved in 6 patients but preservation of function was only achieved in 2 patients.

Neuropsychological Function

Five patients (31.3%) showed neuropsychological deficit before surgery, and the neuropsychological function in the remaining 11 patients (68.8%) was normal. During follow-up, neuropsychological function was preserved in 14 patients (87.5%), improved in 1 patient (6.3%), and deteriorated in 1 patient (6.3%) (Table 2). The patient who had deteriorated neuropsychological function had received previous conventional radiotherapy and showed a gradual decline in neuropsychological function.

Functional Performance Status

Postoperative KPS scores at final follow-up were compared with preoperative KPS scores in 13 patients. Two patients died of unrelated diseases, and 1 patient was lost to follow-up after admission to another hospital with an unrelated disease and thus was not included in this analysis (Table 2). The mean preoperative KPS score was 80.0 (range 60.0–90.0) and the mean postoperative KPS score was 88.3 (range 70.0–90.0). The KPS scores improved in all but 1 patient (Case 2), who died due to radiation necrosis. All patients (except the one who died due to radiation necrosis) returned to their normal daily life and social activities after surgery.

Long-Term Outcome

The recurrence-free survival rate is shown in Fig. 4. The 5-year recurrence-free survival rate in the 16 patients was 86.5% (Fig. 4). The 10-year recurrence-free survival rate was also 86.5% (Fig. 4). The 5-year recurrence-free survival rates were 100.0% after gross-total resection and 68.5% after near-total and subtotal resection (Fig. 5).

Discussion

Craniopharyngiomas located in the retrochiasmatic region are regarded as challenging tumors to remove safely and totally because of their anatomical location and proximity to critical neurovascular structures. Because of the hidden position of retrochiasmatic craniopharyngiomas behind the optic chiasm, their upward extension into the third ventricle, and their downward extension in front of the brainstem, the surgical exposure of these tumors is usually unsatisfactory.[2,20,25,29] Resection of this type of craniopharyngioma has thus been associated with a high rate of surgical mortality, surgical complications, and in-

TABLE 2: Surgical outcomes in 16 patients with tumors resected via the MAPC transpetrosal approach*

					VIS Score						Endocrinological Dysfunction				Neuropsychological Deficit		KPS Score	
					Preop			Postop			Preop		Postop					
Case No.	Approach	Resection	Complication	Recurrence	VA	VF	Total	VA	VF	Total	APH	DI	APH	DI	Preop	Postop	Preop	Postop
1	OZ→TP	GTR	none	no	0	0	0	0	0	0	no	no	no	yes	no	no	90	90
2	TP	STR	none	yes	100	25	100	100	0	100	yes	no	yes	no	no	yes	60	dead†
3	TP	GTR	none	no	28	31	59	2	10	12	no	yes	yes	yes	yes	no	70	dead‡
4	TP→OZ	NTR	none	yes	15	22	37	0	0	0	yes	yes	yes	no	no	no	80	90
5	TP→TSS	GTR	hearing disturbance	no	10	0	10	0	0	0	no	yes	yes	yes	no	no	60	dead‡
6	TP	GTR	none	no	10	10	20	0	0	0	no	no	yes	yes	no	no	80	90
7	TP	NTR	none	no	8	22	30	0	0	0	yes	yes	yes	yes	no	no	80	90
8	TP	GTR	none	no	22	6	28	17	6	23	yes	yes	yes	yes	no	no	80	90
9	TP	NTR	none	no	4	14	18	0	4	4	yes	no	no	no	no	no	80	90
10	TP→OZ	GTR	none	no	20	14	34	0	0	0	yes	yes	yes	yes	yes	yes	80	90
11	TP	NTR	none	no	2	0	2	0	0	0	no	no	no	no	no	no	80	90
12	TP	GTR	none	no	2	22	24	0	22	22	yes	yes	yes	yes	no	no	90	90
13	TP	NTR	none	no	75	22	97		—		yes	no	yes	yes	yes	yes	70	unknown§
14	TP→OZ	NTR	none	no	100	25	100	60	22	82	yes	yes	yes	yes	yes	yes	60	70
15	TP→IH	GTR	none	no	0	18	18	0	0	0	yes	yes	yes	yes	no	no	90	90
16	TP→OZ	GTR	none	no	4	14	18	0	16	16	no	no	yes	yes	yes	yes	90	90

* APH = anterior pituitary hormone; DI = diabetes insipidus; GTR = gross-total resection; NTR = near-total resection; STR = subtotal resection; TP = transpetrosal approach; VA = visual acuity; VF = visual field

† Patient died of radiation necrosis related to the treatment.

‡ Patient died of an unrelated disease.

§ Patient was lost to follow-up.

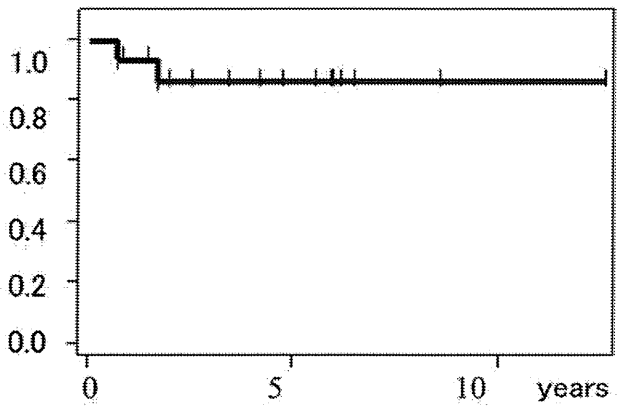

FIG. 4. Recurrence-free survival time (calculated using the Kaplan-Meier method) in patients who underwent surgery for retrochiasmatic craniopharyngiomas via the MAPC transpetrosal approach.

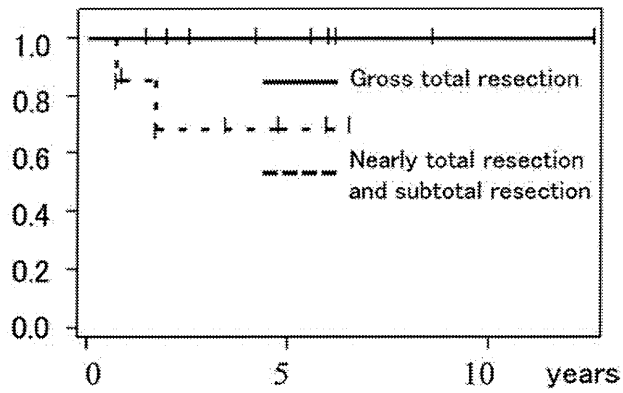

FIG. 5. Recurrence-free survival times (calculated using the Kaplan-Meier method) in relation to the extent of resection in patients who underwent surgery for retrochiasmatic craniopharyngiomas.

complete resection resulting in higher recurrence rates.[6,26] In addition, previous large series of craniopharyngiomas have reported that retrochiasmatic location, larger size, greater than 10% calcification, extension into the third ventricle, and recurrence are significant prognostic factors that negatively affect the extent of resection.[4,6,12,19,21,26,29] Fahlbusch et al. achieved complete resection in only 21.4% of tumors with greater than 10% intratumoral calcification.[6] Several studies have reported that the rate of total resection in repeat surgery is markedly lower than in primary surgery; moreover, perioperative morbidity and mortality are also increased in cases of repeat surgery.[6,12,18,19,26,29] In tumors with posterior extension where the tumor appears to compress the midbrain and pons, most surgeons might recognize that preservation of the membrane of Lilliquist prevents the tumor from adhering to vessels and the brainstem in this area. However, this is less true for recurrent cases. We therefore regarded posterior extension as one of the complicating conditions.

The 16 cases of retrochiasmatic craniopharyngiomas with complicated conditions reported in this series all possessed at least 2 of these risk factors and thus can be regarded as the most challenging subgroup of craniopharyngiomas. Even under such difficult conditions, the results of our MAPC transpetrosal approach were satisfactory in terms of the extent of tumor removal, tumor control, and complication rate. The unique posterior-to-anterior and inferior-to-superior surgical corridor to the retrochiasmatic area afforded by the MAPC transpetrosal approach provides a relatively wide space for surgical procedures in the retrochiasmatic space and offers direct visualization of the posterior and inferior surfaces of the chiasm, the floor of the third ventricle, and the hypothalamic tuber cinereum area. In addition, this posterior-anterior corridor to the chiasm and the third ventricle has the advantage of preserving small perforating vessels from the internal carotid arteries that provide the primary blood supply to the optic chiasm and hypothalamus. These characteristics are distinct from other conventional surgical approaches, such as pterional, orbitozygomatic, and interhemispheric lamina terminalis approaches, and are the primary reason for our good results regarding the extent of tumor removal and preservation of visual function in retrochiasmatic craniopharyngiomas with complicated conditions. The endonasal endoscopic approach can also offer a direct view of the posterior and inferior surfaces of the chiasm, but it is not effective in cases of recurrent tumors, tumors with large calcification, and large tumors because the maneuverability of surgical instruments is not as good as it is when using a microscope, particularly when bipolar forceps are needed for dissection of perforating vessels.[13,16] The endonasal endoscopic approach would thus be unsuitable for the complicated cases reported here.

Despite the effectiveness of the MAPC transpetrosal approach, some considered it to be a time-consuming and difficult procedure that carries a risk of damaging cranial nerves, such as the facial and acoustic nerves, and causing leakage of CSF and surgical-site infection. At our institute, we modified the original transpetrosal approach of Hakuba et al.[11] to overcome these problems and developed the MAPC transpetrosal approach in 1999. In our procedure the dura mater at the middle and posterior fossa is completely peeled off the superior and posterior surfaces of the petrous portion of the temporal bone before the petrosectomy is initiated. This differs from other petrosal approaches and effectively shortens the surgical time for petrosectomy and reduces the extent of bone removal required. For epidural retraction of the temporal and presigmoid dura, a small amount of petrous drilling along the petrous ridge is sufficient to obtain the surgical corridor to the retrochiasmatic space and is also effective in preserving facial and cochlear functions. In fact, hearing was preserved in 15 of the 16 cases and facial function was preserved in all 16 cases. In addition, no surgical-site infection and no leakage of CSF were seen in any of the 16 cases.

A disadvantage of our MAPC transpetrosal approach was an occasional occurrence of transient oculomotor nerve palsy just after the surgical procedure, but we consider this an acceptable complication considering the surgical difficulty of the cases. Seven patients underwent 2-staged operations involving the transpetrosal approach and another approach. One of the reasons for a second operation was that in cases with adhesions between the tu-

mor and the perforator of the opposite internal carotid artery, these parts of the tumor are more difficult to remove safely via the transpetrosal approach. However, these parts could be removed safely using an orbitozygomatic approach from the contralateral side. Another reason is that the part of the sella turcica or the superoposterior part of the third ventricle is more difficult to access directly because the transpetrosal approach provides inferior-to-superior and posterior-to-anterior projections. However, the residual tumors in the sella turcica could be removed safely via transsphenoidal surgery and residual tumors in the superoposterior part of the third ventricle could be removed using an interhemispheric approach.

There is a school of thought that retrochiasmatic craniopharyngiomas with complicated conditions should be treated conservatively with a combination of safe partial resection and stereotactic radiosurgery to reduce the risks of surgery. This conservative treatment has provided acceptable results for some types of craniopharyngiomas.[14,24,25,27] However, of the cases presented in this report, radiotherapies or radiosurgeries had already been applied in 4 cases; radiotherapies or stereotactic radiosurgeries were not acceptable in the other 12 cases because of the proximity of the tumors to the optic chiasm and hypothalamus. In general, radiosurgery is contraindicated if the distance between the tumor and optic apparatus is less than 3 mm because the visual pathways would typically receive more than 10 Gy in these situations.[14] The 16 cases of retrochiasmatic craniopharyngiomas presented in this report could be considered the most difficult cases to control, and radical resection of the tumor should be regarded as the last treatment. Our results regarding extent of tumor removal, tumor control, complication rate, and visual function were satisfactory compared with the other reports of craniopharyngiomas.[4,6,12,19,21,26,29]

Conclusions

Although this represents the first report on surgical outcomes of the transpetrosal approach for retrochiasmatic craniopharyngiomas, we achieved satisfactory results using the MAPC transpetrosal approach for the removal of retrochiasmatic craniopharyngiomas under complicated conditions. The MAPC transpetrosal approach can provide an alternative procedure for resection of retrochiasmatic craniopharyngiomas with complicated conditions such as recurrence, history of radiation, large calcification, large tumor diameter, and extreme superior and posterior extension.

Disclosure

The authors report no conflict of interest concerning the materials or methods used in this study or the findings specified in this paper.

Author contributions to the study and manuscript preparation include the following. Conception and design: Kunihiro, Goto, Ohata. Acquisition of data: Kunihiro, Goto, Ishibashi. Analysis and interpretation of data: Kunihiro. Drafting the article: Kunihiro. Critically revising the article: Goto.

References

1. Al-Mefty O, Ayoubi S, Kadri PA: The petrosal approach for the total removal of giant retrochiasmatic craniopharyngiomas in children. **J Neurosurg 106 (2 Suppl):**87–92, 2007
2. Ammirati M, Samii M, Sephernia A: Surgery of large retrochiasmatic craniopharyngiomas in children. **Childs Nerv Syst 6:**13–17, 1990
3. Dehdashti AR, de Tribolet N: Frontobasal interhemispheric trans-lamina terminalis approach for suprasellar lesions. **Neurosurgery 56 (2 Suppl):**418–424, 2005
4. Duff J, Meyer FB, Ilstrup DM, Laws ER Jr, Schleck CD, Scheithauer BW: Long-term outcomes for surgically resected craniopharyngiomas. **Neurosurgery 46:**291–305, 2000
5. Fahlbusch R, Hofmann BM: Surgical management of giant craniopharyngiomas. **Acta Neurochir (Wien) 150:**1213–1226, 2008
6. Fahlbusch R, Honegger J, Paulus W, Huk W, Buchfelder M: Surgical treatment of craniopharyngiomas: experience with 168 patients. **J Neurosurg 90:**237–250, 1999
7. Fahlbusch R, Schott W: Pterional surgery of meningiomas of the tuberculum sellae and planum sphenoidale: surgical results with special consideration of ophthalmological and endocrinological outcomes. **J Neurosurg 96:**235–243, 2002
8. Fatemi N, Dusick JR, de Paiva Neto MA, Malkasian D, Kelly DF: Endonasal versus supraorbital keyhole removal of craniopharyngiomas and tuberculum sellae meningiomas. **Neurosurgery 64 (5 Suppl 2):**269–286, 2009
9. Folstein MF, Folstein SE, McHugh PR: "Mini-mental state". A practical method for grading the cognitive state of patients for the clinician. **J Psychiatr Res 12:**189–198, 1975
10. Golshani KJ, Lalwani K, Delashaw JB Jr, Selden NR: Modified orbitozygomatic craniotomy for craniopharyngioma resection in children. Clinical article. **J Neurosurg Pediatr 4:**345–352, 2009
11. Hakuba A, Nishimura S, Inoue Y: Transpetrosal-transtentorial approach and its application in the therapy of retrochiasmatic craniopharyngiomas. **Surg Neurol 24:**405–415, 1985
12. Karavitaki N, Brufani C, Warner JT, Adams CBT, Richards P, Ansorge O, et al: Craniopharyngiomas in children and adults: systematic analysis of 121 cases with long-term follow-up. **Clin Endocrinol (Oxf) 62:**397–409, 2005
13. Kim EH, Ahn JY, Kim SH: Technique and outcome of endoscopy-assisted microscopic extended transsphenoidal surgery for suprasellar craniopharyngiomas. Clincal article. **J Neurosurg 114:**1338–1349, 2011
14. Lee M, Kalani MY, Cheshier S, Gibbs IC, Adler JR, Chang SD: Radiation therapy and CyberKnife radiosurgery in the management of craniopharyngiomas. **Neurosurg Focus 24(5):**E4, 2008
15. Liu JK, Christiano LD, Gupta G, Carmel PW: Surgical nuances for removal of retrochiasmatic craniopharyngiomas via the transbasal subfrontal translamina terminalis approach. **Neurosurg Focus 28(4):**E6, 2010
16. Liu JK, Christiano LD, Patel SK, Eloy JA: Surgical nuances for removal of retrochiasmatic craniopharyngioma via the endoscopic endonasal extended transsphenoidal transplanum transtuberculum approach. **Neurosurg Focus 30(4):**E14, 2011
17. Maira G, Anile C, Colosimo C, Cabezas D: Craniopharyngiomas of the third ventricle: trans-lamina terminalis approach. **Neurosurgery 47:**857–865, 2000
18. Minamida Y, Mikami T, Hashi K, Houkin K: Surgical management of the recurrence and regrowth of craniopharyngiomas. **J Neurosurg 103:**224–232, 2005
19. Mortini P, Losa M, Pozzobon G, Barzaghi R, Riva M, Acerno S, et al: Neurosurgical treatment of craniopharyngioma in adults and children: early and long-term results in a large case series. Clinical article. **J Neurosurg 114:**1350–1359, 2011
20. Rutka JT: Editorial. Craniopharyngioma. **J Neurosurg 97:**1–2, 2002
21. Shi XE, Wu B, Fan T, Zhou ZQ, Zhang YL: Craniopharyngioma: surgical experience of 309 cases in China. **Clin Neurol Neurosurg 110:**151–159, 2008

22. Shibuya M, Takayasu M, Suzuki Y, Saito K, Sugita K: Bifrontal basal interhemispheric approach to craniopharyngioma resection with or without division of the anterior communicating artery. **J Neurosurg 84:**951–956, 1996
23. Shirane R, Ching-Chan S, Kusaka Y, Jokura H, Yoshimoto T: Surgical outcomes in 31 patients with craniopharyngiomas extending outside the suprasellar cistern: an evaluation of the frontobasal interhemispheric approach. **J Neurosurg 96:**704–712, 2002
24. Smee RI, Williams JR, Kwok B, Teo C, Stening W: Modern radiotherapy approaches in the management of craniopharyngiomas. **J Clin Neurosci 18:**613–617, 2011
25. Stripp DC, Maity A, Janss AJ, Belasco JB, Tochner ZA, Goldwein JW, et al: Surgery with or without radiation therapy in the management of craniopharyngiomas in children and young adults. **Int J Radiat Oncol Biol Phys 58:**714–720, 2004
26. Van Effenterre R, Boch AL: Craniopharyngioma in adults and children: a study of 122 surgical cases. **J Neurosurg 97:**3–11, 2002
27. Veeravagu A, Lee M, Jiang B, Chang SD: The role of radiosurgery in the treatment of craniopharyngiomas. **Neurosurg Focus 28(4):**E11, 2010
28. Wechsler D: WAIS-III: **Administration and Scoring Manual: Wechsler Adult Intelligence Scale, ed 3.** San Antonio, TX: Psychological Corp, 1997
29. Yaşargil MG, Curcic M, Kis M, Siegenthaler G, Teddy PJ, Roth P: Total removal of craniopharyngiomas. Approaches and long-term results in 144 patients. **J Neurosurg 73:**3–11, 1990

Manuscript submitted April 4, 2013.
Accepted October 3, 2013.
Please include this information when citing this paper: published online November 15, 2013; DOI: 10.3171/2013.10.JNS13673.
Address correspondence to: Noritsugu Kunihiro M.D., Department of Neurosurgery, Osaka City University Graduate School of Medicine, 1-4-3 Asahi-machi, Abeno-ku, Osaka 545-8585, Japan. email: nori9216@med.osaka-cu.ac.jp.

Biomaterials 35 (2014) 3396–3405

Contents lists available at ScienceDirect

Biomaterials

journal homepage: www.elsevier.com/locate/biomaterials

The acceleration of boron neutron capture therapy using multi-linked mercaptoundecahydrododecaborate (BSH) fused cell-penetrating peptide

Hiroyuki Michiue [a,*], Yoshinori Sakurai [b], Natsuko Kondo [b], Mizuki Kitamatsu [c], Feng Bin [d], Kiichiro Nakajima [e], Yuki Hirota [f], Shinji Kawabata [f], Tei-ichi Nishiki [a], Iori Ohmori [a], Kazuhito Tomizawa [g], Shin-ichi Miyatake [f], Koji Ono [b], Hideki Matsui [a]

[a] Department of Physiology, Okayama University Graduate School of Medicine, Dentistry and Pharmaceutical Sciences, 2-5-1 Shikata-cho, Kita-Ku, Okayama City, Okayama 700-8558, Japan
[b] Particle Radiation Oncology Research Center, Research Reactor Institute, Kyoto University, Kumatori-cho, Osaka 590-0494, Japan
[c] Department of Applied Chemistry, Faculty of Science and Engineering, Kinki University, 3-4-1 Kowakae, Higashi-Osaka City, Osaka 577-8502, Japan
[d] Department of Biotechnology, Dalian Medical University, No. 9 West Section, Lvshun South, Dalian 116044, China
[e] KNC Laboratories, Ltd., 1-1-1, Murotani, Nishi-ku, Kobe City, Hyogo 651-2241, Japan
[f] Department of Neurosurgery, Osaka Medical College, 2-7 Daigaku-machi, Takatsuki City, Osaka 569-8686, Japan
[g] Department of Molecular Physiology, Faculty of Life Sciences, Kumamoto University, 1-1-1 Honjou, Kumamoto City, Kumamoto 860-8556, Japan

ARTICLE INFO

Article history:
Received 4 December 2013
Accepted 19 December 2013
Available online 20 January 2014

Keywords:
Protein transduction
BSH poly-arginine
TAT
Oron neutron capture therapy (BNCT)

ABSTRACT

New anti-cancer therapy with boron neutron capture therapy (BNCT) is based on the nuclear reaction of boron-10 with neutron irradiation. The median survival of BNCT patients with glioblastoma was almost twice as long as those receiving standard therapy in a Japanese BNCT clinical trial. In this clinical trial, two boron compounds, BPA (boronophenylalanine) and BSH (sodium borocaptate), were used for BNCT. BPA is taken up into cells through amino acid transporters that are expressed highly in almost all malignant cells, but BSH cannot pass through the cell membrane and remains outside the cell. We simulated the energy transfer against the nucleus at different locations of boron from outside the cell to the nuclear region with neutron irradiation and concluded that there was a marked difference between inside and outside the cell in boron localization. To overcome this disadvantage of BSH in BNCT, we used a cell-penetrating peptide system for transduction of BSH. CPP (cell-membrane penetrating peptide) is very common peptide domains that transduce many physiologically active substances into cells *in vitro* and *in vivo*. BSH-fused CPPs can penetrate the cell membrane and localize inside a cell. To increase the boron ratio in one BSH-peptide molecule, 8BSH fused to 11R with a dendritic lysine structure was synthesized and administrated to malignant glioma cells and a brain tumor mouse model. 8BSH-11R localized at the cell nucleus and showed a very high boron value in ICP results. With neutron irradiation, the 8BSH-11R administrated group showed a significant cancer killing effect compared to the 100 times higher concentration of BSH-administrated group. We concluded that BSH-fused CPPs were one of the most improved and potential boron compounds in the next-stage BNCT trial and 8BSH-11R may be applied in the clinical setting.

1. Introduction

For decades, malignant glioma, especially glioblastoma (GBM) was not curable, but in 2004, a randomized phase III trial by the European Organization for the Research and Treatment of Cancer (EORTC) and the National Cancer Institute of Canada Clinical Trials Group (NCIC) reported improved median and 2-year survival of patients with glioblastoma treated with concomitant and adjuvant temozolomide (TMZ) and radiotherapy [1]. The median survival was 14.6 months with radiotherapy plus TMZ and 12.1 months with radiotherapy alone. Furthermore, recently, the Japanese boron neutron capture therapy (BNCT) group against malignant brain tumor reported that the median survival of newly-diagnosed glioblastoma patients with BNCT was 23.5 months [2]. This BNCT outcome is excellent and hopeful for malignant glioma patients.

* Corresponding author. Tel.: +81 86 235 7105; fax: +81 86 235 7111.
E-mail address: hmichiue@md.okayama-u.ac.jp (H. Michiue).

0142-9612/$ – see front matter © 2013 Elsevier Ltd. All rights reserved.
http://dx.doi.org/10.1016/j.biomaterials.2013.12.055

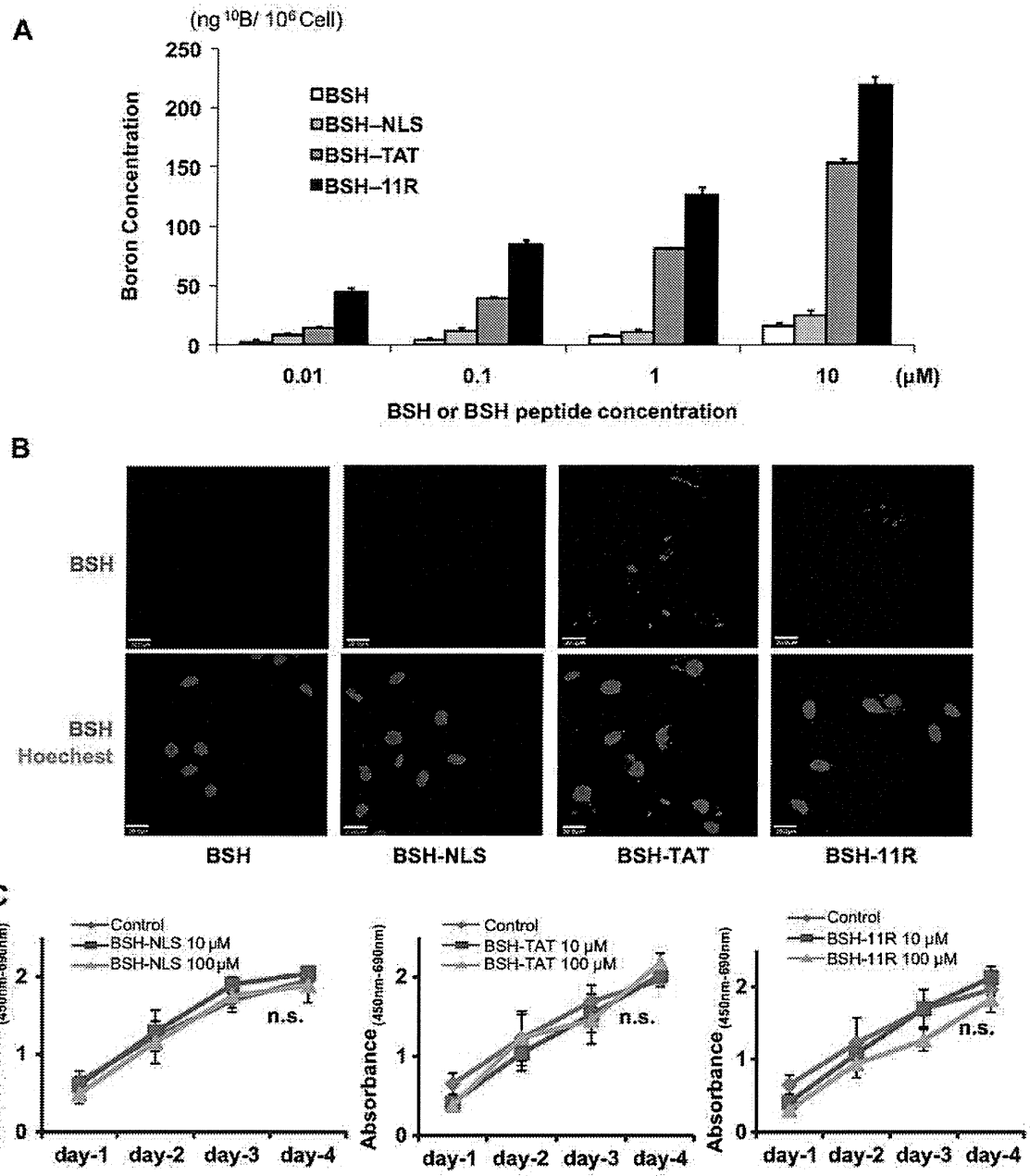

Fig. 1. Administration of BSH-peptide into U87 delta EGFR cell and evaluation of intra-cellular function 1-A: Boron concentration of U87 delta EGFR cells administrated different kinds of BSH and BSH-peptide at 0.01, 0.1, 1 and 10 μM for 12 h. 1-B: Immunocytochemistry showing BSH (red) and nucleus (blue) with identified BSH antbody and Hoechst 33342 by confocal microscopy. Scale bar = 20 μm 1-C: Three graphs showing cell proliferation after administration of each BSH or BSH-peptide at 10 or 100 μM for 4 days by the measurement of absorbance (450 nm-690 nm) with WST-1 reagent. (For interpretation of the references to colour in this figure legend, the reader is referred to the web version of this article.)

BNCT is based on the nuclear capture and fission reactions that occur when boron-10, a non-radioactive isotope and a constituent of natural elemental boron, is irradiated with low energy (<0.025 eV) thermal neutrons (*n*th) to produce high energy (2.3 MeV) alpha (α) particles and recoiling lithium-7 nuclei ($^{10}B + nth \rightarrow [^{11}B] \rightarrow {}^4He(\alpha) + {}^7Li + 2.38$ MeV) [3,4]. BNCT has been used to treat patients with high-grade primary brain tumors and a much smaller number of patients with other types of brain tumors [2,5,6]. For BNCT to be successful, there must be high uptake of ^{10}B by the tumor and low levels in the normal brain, and sufficient fluence of thermal neutrons must be delivered to the tumor. In their BNCT, two low molecular weight ^{10}B-containing drugs, boronophenylalanine (BPA) and/or sodium borocaptate (BSH), were used as capture agents [7]. Two boron compounds have been used clinically: sodium undecahydro-mercaptocloso-dodecaborate ($Na_2B_{12}H_{11}SH$, also referred to as sodium borocaptate or 'BSH') in Japan and Europe and 4-dihydroxyborylphenylalanine (boronophenylalanine or 'BPA') in the United States [4,8]. BPA can enter and accumulate in malignant cells, but BSH shows leakage from the tumor area and cannot transduce into cells [4]. The nuclear reaction caused by BNCT outside cells is mildly effective against malignant cells, but a precise simulation dependent on the intracellular

localization of the boron compound has not been performed. To overcome this weakness of BSH, several drug delivery systems (DDS) have been reported using therapeutically useful doses of BSH-containing pharmacophores [9]. Protein transduction therapy with cell-membrane penetrating peptides (CPPs) and a protein/peptide transduction domain (PTD) has marked advantages to get several materials (e.g. protein, peptide, small-interfering RNA) into cells without toxicity *in vitro* and *in vivo* [10–15]. Well-known intracellular transduction domain peptides, including the HIV trans-activator of transduction (TAT; aa 48–60 or 47–57), polyarginine domain (11R and R9), antennapedia (Antp; aa 43–58) etc; have been reported as CPPs and PTD [16]. The mechanism of intracellular delivery using these peptide domains is proposed as a three-step process: first, binding of the CPPs to the cellular membrane with electrical interaction between CPPs and the cell membrane; second, stimulation of intracellular uptake by macropinocytosis; and third, release from macropinosomes into the cytoplasm [17].

In this time, we will try to prove that the intracellular localization of the boron compound is a marked advantage in BNCT and CPPs could be applied as a delivery system to carry a boron compound (BSH) into malignant glioma cells *in vitro* and *in vivo* for BNCT.

2. Materials and methods

2.1. Simulations of energy deposition in the nucleus for the local distribution of ^{10}B in one cell

There have been some previous works on the estimation of energy deposition at the cell level for BNCT [18–20]. Referring to these previous works, the influence of energy deposition in the cell nucleus for the local distribution of ^{10}B in a cell was assessed using analytical and stochastic methods. Fig. 1-A shows the geometry and mathematical expression for this assessment. The shapes of the cell and cell nucleus were supposed to be spherical. The contributions from ^{10}B distributed outside and inside of the nucleus were assessed separately. For the contribution from outside ^{10}B, the probabilities of the alpha particle and ^{7}Li nucleus generated due to $^{10}B(n,\alpha)^{7}Li$ were calculated geometrically for the incidence in the nucleus at a certain angle. The particle energy, for entering and exiting the cell nucleus, was calculated for each angle, considering the stopping powers [21,22]. The difference of these particle energies was regarded as the deposited energy in the cell nucleus.

For the contribution from inside ^{10}B, the probabilities of the generated particles for going forward in a certain direction were calculated geometrically. The energy lost until the particle exited the cell nucleus was calculated considering the stopping power. This lost energy was regarded as the deposited energy in the cell nucleus.

Integrating the above-calculated energy depositions into the weight of the angle and the ^{10}B distribution, the average energy deposition in the cell nucleus due to a $^{10}B(n,\alpha)^{7}Li$ reaction was estimated. Here, assessments were performed for five conditions of ^{10}B distribution; ① uniformly distributed in the whole cell, ② locally distributed only in the cell membrane, ③ uniformly distributed in cytoplasm, ④ locally distributed only in the nuclear membrane, and ⑤ uniformly distributed in the cell nucleus. The radius of the cell was fixed at 5 μm, and the radius of the cell nucleus was varied among 2, 2.5 and 3 μm.

2.2. Glioma cell lines

U87 DEGFR and PA U87 glioma cell lines (kindly donated by Professor Cavenee and Dr. Mukasa of the University of California at San Diego) were used in all experiments. U87 DEGFR cells stably express constitutively active EGFR, EGFRvIII, whereas PAU 87 cells not overexpress EGFR. The cells were maintained in Dulbecco's modified Eagle's medium (DMEM) (Invitrogen) with 10% fetal bovine serum (FBS), penicillin and streptomycin at 37 °C in a humidified atmosphere containing 5% CO_2.

2.3. Cell proliferation assay (WST-1 assay)

Cell Viability Assay—Cell viability was determined using a WST-1 assay (Roche Applied Science) as described previously [11]. After glioma cells (1×10^3/well) were seeded in 96-well flat-bottomed plates, they were cultured in Dulbecco's modified Eagle's medium containing 10% FBS for 24 h. The cells were then supplemented with various concentrations of BSH or BSH-peptide and further incubated for 24 h (day 1), 48 h (day 2), 72 h (day 3) and 96 h (day 4). Cell viability was measured using the WST-1 assay each day according to the manufacturer's instructions (Roche Applied Science).

2.4. Immunohistochemical analysis (IHC) and measurement of ^{10}B content in vitro

IHC was carried out to analyze the distribution of BSH *in vitro*. Cells were incubated for 1 h, 3 h, 6 h and 24 h with BSH and BSH-peptide. After incubation of boron compounds, the cells were thoroughly washed with PBS twice, fixed with 4% paraformaldehyde (PFA) for 10 min, and then incubated with anti-BSH mouse mAb [24]. The secondary antibody was Cy3 or Cy5-conjugated mouse IgG. Fluorescence signals were observed using a confocal laser microscope (FluoView; Olympus, Japan). To detect ^{10}B in cells, BSH or BSH-peptides were added to 6-cm dishes. After 2 h, 8 h and 24 h of incubation, the cells were washed with PBS, dissolved in 200 μL concentrated nitric acid overnight, and diluted with 5 mL MillQ water. The ^{10}B content was measured by inductively coupled plasma-atomic emission spectrometry (ICP-AES, Vista Pro, Seiko Instruments; Japan) as described previously [23,24].

2.5. Brain tumor model and detection of BSH-peptide in vivo

U87 ΔEGFR cells (3×10^5 cells/5 μL) were injected into the striatum of female 4–6 week-old nude mice (15–20 g, BALB/c Slc-nu/nu; Japan SLC) as described [24]. After two weeks, boron 0.7 mg-boron/200 μL of 8BSH-peptide or BSH was administered into tumor-bearing mice intravenously via the tail. After 6 h and 24 h, the mice were sacrificed and the brains were placed in PBS. Sections of 10-μm thickness were cut on a microtome (CM 1850; Leica Microsystems, Wetzlar, Germany). IHC was carried out as described previously and observed with a confocal laser microscopy [23,24].

2.6. Multi BSH-peptide synthesis

BSH was purchased from Katchem (Prague, Czech Republic) and all BSH-peptides were synthesized at KNC Laboratories Co. Ltd (Kobe, Japan).

2.6.1. $[Cys(Npys)]_8$-$(Lys)_7$-Arg-Arg-Arg-Arg-Arg-Arg-Arg-Arg-Arg-Arg-Arg-Arg-NH_2

The desired fully protected peptides resin was assembled using an Applied Biosystems model 433 peptide synthesizer with Fmoc-NH-SAL-PEG resin (0.18 mmol/g, 0.25 mmol) as the starting solid support, as shown in Fig 3. Fmoc-Arg(Pbf), Fmoc-Lys(Fmoc), Boc-Cys(Npys) were used as amino acid materials The obtained $[Boc\text{-}Cys(Npys)]_8\text{-}(Lys)_7\text{-}Arg(Pbf)_{11}$-NH-SAL-PEG resin was treated with the usual deprotecting reagents (TFA-TIS-H_2O (95/2.5/2.5/v/v)) at room temperature for 2 h. The desired crude S-Npys title peptide derivatives were isolated and purified by RP-HPLC.

2.6.2. $[Cys(BSH)]_8$-$(Lys)_7$-Arg-Arg-Arg-Arg-Arg-Arg-Arg-Arg-Arg-Arg-Arg-Arg-NH_2

To a solution of S-Npys peptide (35 mg 7.46 μmol) in water-CH3CN-DMSO (6/1/3 ml) was added solid $B_{12}SH^-$ 2Na (11.6 mg, 54.9 μmol) and stirred at room temperature for 6 h. The reaction mixture was then directly applied to the following preparative HPLC purification procedure. The purified titled BSH peptide was obtained as 13.4 mg (37.6% yield) as the lyophilized TFA salt products.

RP-HPLC Purity: 98.7%, MW:4771.95 (C132H355B96N67O26S10),m/z 1592.4 ($[M+3H]^{3+}$ 1591.7), m/z 328.7 ($[M+TFA+15H]^{15+}$ 326.7), m/z279.4 ($[M+17H]^{17+}$ 281.7)

Cys(BSH)-Arg11-NH_2

Cys(BSH)-Arg-Arg-Arg-Arg-Arg-Arg-Arg-Arg-Arg-Arg-Arg-NH_2, MW:2001.37, C69H152B12N4612S2, MS : m/z 668.4 ([M+3H]3+668.13, m/z 706.5 ([M+TFA+3H]3+706.14 m/z 782.3 ([M+3TFA+3H]3+782.16

Cys(BSH)-Lys[Cys(BSH)-]Arg11-NH_2

Cys(BSH)-Lys[Cys(BSH)-]-Arg-Arg-Arg-Arg-Arg-Arg-Arg-Arg-Arg-Arg-Arg-NH_2

MW : 2394.1 C78H177B24 N49O14 S4, MS : m/z398.9 (M+12H.)12+ 398.7

[Cys(BSH)]4-(Lys)3-Arg11-NH_2

[Cys(BSH)]8-(Lys)7-Arg-Arg-Arg-Arg-Arg-Arg-Arg-Arg-Arg- Arg-Arg-Arg-NH_2

MW : 3181.4 C98H231B48N55O18 S8, MS : m/z 399.4 ([M+8H]8+ 398.7, m/z376.2 (M+5TFA+10H.)10+ 376.1

2.7. Cell proliferation assay with neutron radiation in research reactor

U87 delta EGFR cells were incubated with 0.1, 1, or 10 μM 8BSH-11R or 0.8, 8, 80, 800, or 8000 μM BSH for 6 h at 37 °C and 5% CO_2 in an incubator. After the incubation of boron compounds, glioma cells were washed with PBS twice and then irradiated with neutrons in Kyoto University research reactor (KUR) for 30 min (1 MW, rate of thermal neutron fluence 2.9–3.7 × 10^{12}/cm^2, rate of epithermal neutron fluence 5.2–6.5 × 10^{11}/cm^2). After irradiation, to check the early-stage BNCT reaction, the cells were separated into 3000 cells per well in a 96-well plate (each group $n = 6$) with culture medium and the WST-1 assay was performed 24 h and 48 h after neutron irradiation. To evaluate the late-stage BNCT effect, 5000 cells per 35 mm dish (each group $n = 6$) were cultured for 2 weeks and evaluated by colony formation assay with methanol fixation and 2% Giemsa solution staining [25].

2.8. Statistical analysis

Data are shown as the mean ± S.D. Data were analyzed using Student's *t*-test to compare the two conditions, and $p < 0.05$ was considered significant.

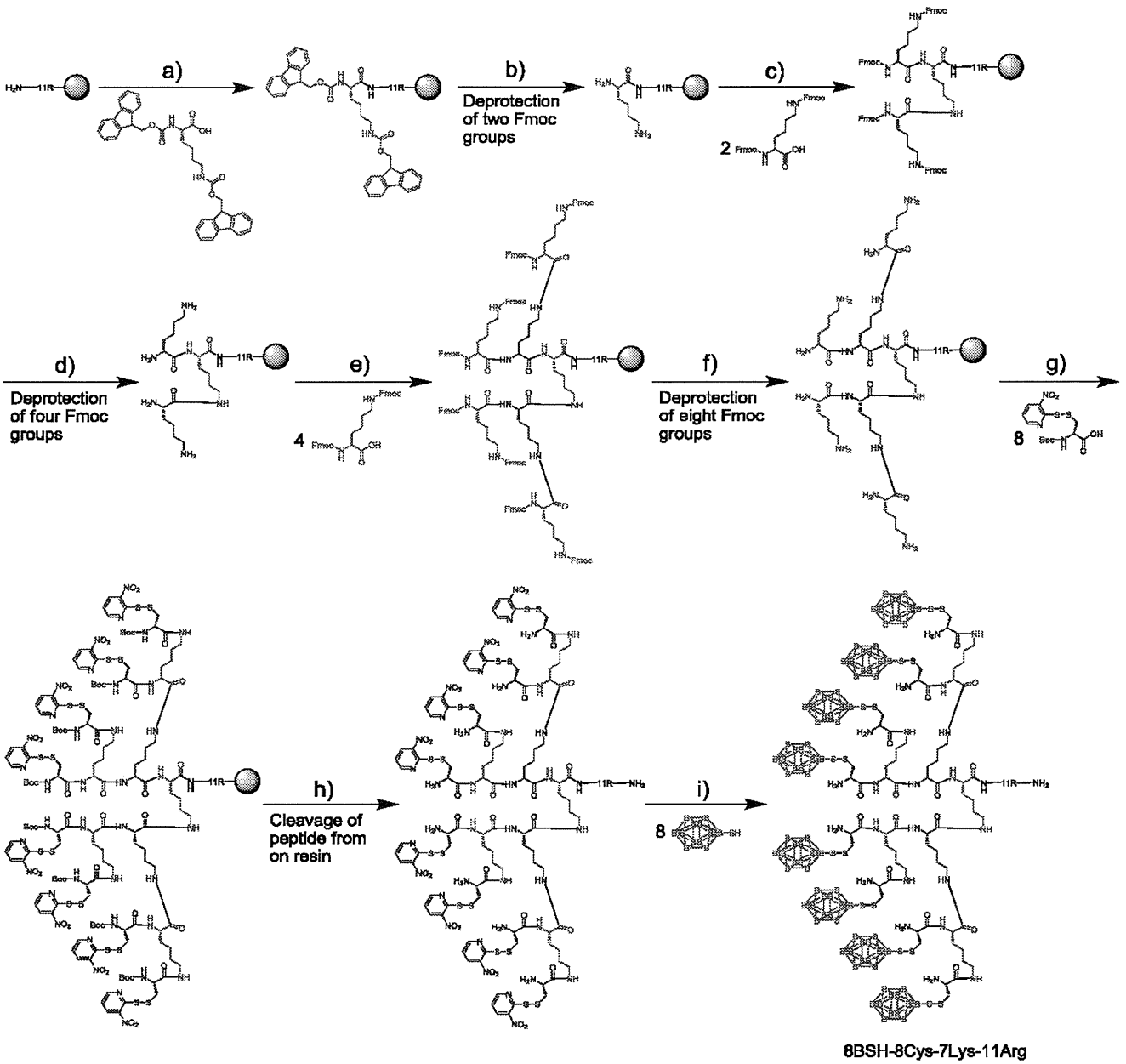

Fig. 2. Synthetic route of 8BSH-8Cys-7Lys-11Arg. Starting material is resin containing amino groups on the surface. a),c),e) Fmoc-Lys(Fmoc)(2eq), coupling reagents: HBTU, HOBt(2eq each),DIEA(4eq)/NMP; b),d),f) 20% piperidine/NMP; g) Boc-Cys(Npys)(4eq), coupling reagent DIC(4eq)/NMP; h) Trifluoroacetic acid/water/triisopropylsilane (=95/2.5/2.5 v/v/v); i) BSH.

3. Results

3.1. Simulations of changes in the energy deposition at one cell level for the radius of the cell nucleus

Suppl. Fig. 1 and Table 1 show the energy transfer ratio to the cell nucleus for the cell and nucleus radii. In Suppl. Fig. 2, the three curves correspond to three of the above-mentioned ^{10}B distributions, such as uniformly in the cell, cytoplasm only and nucleus only, forcell radii of 5, 7.5 and 10 μm. Under all distribution conditions, the average ^{10}B concentration in the whole cell was equal to 1 ppm. For any cell-nucleus radius, the energy deposition was normalized for local distribution only in the cytoplasmic membrane to 100%, because the boron compound of BSH cannot penetrate the cell membrane and we aimed to show the different effectiveness of an inside-cell or outside-cell boron compound with neutron irradiation.

It was found that the energy deposition markedly decreased when ^{10}B was not taken up into or near the cell nucleus, even for the same average ^{10}B concentration in the whole cell. As the cell nucleus is smaller, the effect of ^{10}B localization to the cell nucleus is larger. In the comparison of the absolute values, the energy deposition in the nucleus relatively increased as the cell nucleus became larger, for any condition of ^{10}B distribution. These three curves correspond to three of the above-mentioned ^{10}B distributions. Under any distribution condition, the average ^{10}B concentration in

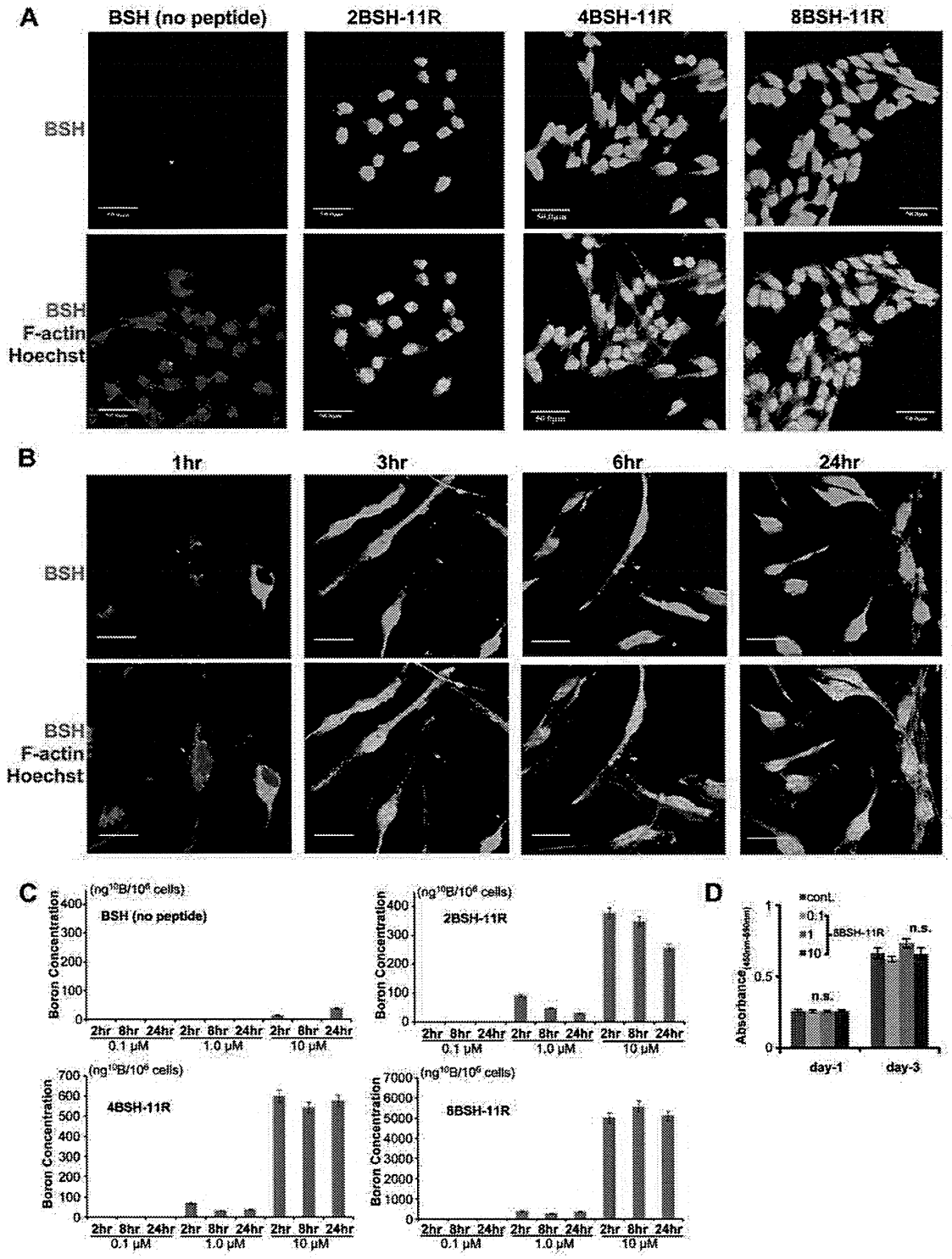

Fig. 3. BSH localization in glioma cells and boron ICP results of multi-BSH-11R (2BSH, 4BSH and 8BSH) 3-A: Confocal imaging of U87 delta EGFR cells showing BSH localization (green), cytoplasm (f-actin, red) and nucleus (Hoechst, blue) with 10 μM BSH, 2BSH-11R, 4BSH-11R and 8BSH-11R intracellular BSH localization in U87 delta EGFR cells for 12 h. Scale bar = 50 μm. 3-B: Immunocytochemistry showing BSH (green), f-actin (red), nucleus (blue) 1, 3, 6, and 24 h after administration of 10 μM 8BSH-11R. 3-C: ICP results showing B10 concentration in U87 delta EGFR cells with 0.1, 1, 10 μM BSH or BSH-peptide 2, 8, and 24 h after administration for ngB^{10} per 10^6 cells. 3-D: Cell proliferation results of U87 delta EGFR cells with control, 0.1, 1.0 and 10 μM 8BSH-11R for 1 or 3 days measured with WST-1 for absorbance (450 nm-690 nm). (For interpretation of the references to colour in this figure legend, the reader is referred to the web version of this article.)

Table 1
Calculated value of the local energy transfer ratio against nucleus % cytoplasm-membrane control from Fig. 1.

Cell radius (μm)	Nucleus radius (μm)	Energy transfer ratio to nucleus (% cytoplasm-membrane control)				
		Nucleus only	Nuclear-membrane only	Cytoplasm only	Cytoplasm-membrane only	Uniformly distributed
5	2.5	3370	900	317	100	592
7.5	2.5	13,100	3490	371	100	827
7.5	5	2090	570	206	100	746
10	2.5	104,000	27,700	1420	100	2990
10	5	9320	2540	458	100	1540
10	7.5	1940	507	205	100	917

the whole cell was equal to 1 ppm. For any cell-nucleus radius, the energy deposition was normalized to the uniform distribution in the whole cell to 100%.

In particular, Table 1 shows that the energy transfer ratio to the nucleus in nucleus-only localization was almost 30–1000 times different form cytoplasm membrane localization. Boron localization in the cytoplasm membrane control led the outside cell localization and outside cell-to-cell space in an *in vivo* model.

3.2. Intracellular BSH localization and boron concentration of glioma cells administrated BSH-fused peptide

BSH-peptide was produced with S–S connection between peptidesCys-NPYS and SH of BSH. The administration of BSH-fused CPPs (TAT:GRKKRRQRRR and 11R:RRRRRRRRRRR) to glioma cells showed high boron concentration according to the amount of administrated BSH-CPPs (Fig. 1-A), and BSH was clearly observed in U87 delta EGFR cells in the cytoplasmic region but not in the nuclear area (Fig. 1-B). On the other hand, BSH and BSH-NLS (NLS: PKKKRKV) administrated glioma cells did not demonstrate BSH inside the cell on immunohistochemistry with BSH antibody. The intracellularly transduced BSH was not toxic to glioma cells in the WST-1 assay for 4 days (Fig. 1-C).

3.3. Synthesis of 8BSH-8Cys-7Lys-11Arg (8BSH-11R)

The 8BSH-8Cys-7Lys-11Arg (8BSH-11R) was synthesized by disulfide linkage between the Cys(Npys)-activated cell-penetrating peptide (CPP) containing a peptide dendrimer and the BSHs after the CPP was prepared by Fmoc-based solid-phase peptide synthesis (SPPS) [26]. The sequence of peptide moiety is N′-Lys(Lys(Lys(H-Cys(Npys)2)2)2)-Arg11-NH_2-C′; Npys = 3-nitro-2-pyridinesulfenyl group. The synthesis route of 8BSH-11R is shown in Fig. 2. The structure contains multiple boron clusters and one CPP, and such a dendritic structure containing one CPP has seldom been reported [27].

3.4. Transduction of multi-BSH fused CPP into malignant glioma cells

BSH-11R could enter glioma cells, but was localized in the cytoplasm. BSH-11R's boron content ratio was only a few percentage of total molecular weight. To improve the boron content in one BSH-peptide, multi-BSH-fused CPPs (2BSH, 4BSH, and 8BSH) were synthesized. After administration, all multi-BSH fused 11R could enter cells and almost all was localized in the nucleus (Fig. 3-A). The time course imaging of 8BSH-11R-administrated glioma shows the change from cytoplasmic localization (1 h) to whole cell existence (3 h and 6 h) (Fig. 3-B). In particular 24 h after administration, almost all BSH was localized in the nucleus. Malignant glioma cells administrated with each multi-BSH-11R (2BSH-11R, 4BSH-11R, 8BSH-11R) showed a high concentration of intracellular boron concentration in direct proportion to the number of connected BSH in ICP results (Fig. 3-C, Table 2). In the 10 μM 8BSH-11R group, the boron content amount was almost 5000 ppm in 10^6 cells. Despite using a high-concentration BSH-peptide, this was no toxicity to the cells (Fig. 3-D).

3.5. In vivo 8BSH-11R distribution in intracranial brain tumor model

U87 delta EGFR glioma cells were implanted into a nude mouse brain and, after two weeks, 8BSH-11R was injected through the tail vein [23,24]. These mice were sacrificed 6 h and 24 h after the injection. Human GFAP antibody specifically stained only human GFAP that showed U87 delta EGFR cells. In low magnification results, 8BSH-11R was localized in the tumor and peripheral tumor area (Fig. 4-A). Almost all 8BSH-11R was co-localized with human glioma cells at 6 h and 24 h. In high magnification observation, 8BSH-11R had definitely transduced into the tumor center and tumor edge, but not into the normal brain at 6 h and 24 h (Fig. 4-B, C). 8BSH-11R in the tumor area and at the tumor edge could enter cells and was localized in the nucleus and cytoplasm. On the other hand, 8BSH-11R could not be detected in the normal brain area on high magnification confocal microscopy (Fig. 4-B, C).

3.6. BNCT effect after neutron irradiation with BSH or 8BSH-11R against malignant glioma

8BSH-11R or BSH was administrated to glioma cells at the point of equalization of boron content. With neutron radiation for 30 min, 1 kW (thermal neutron fluence $3.2 \times 101^2/cm^2$) at Kyoto University Reactor Institute, after neutron irradiation, early-stage (24 h and 48 h after neutron radiation) and late-stage (2 weeks after neutron radiation) BNCT effects were evaluated separately with the WST-1 assay and colony formation assay. As early effects on cell proliferation, the 1 μM- and 10 μM- administrated 8BSH-11R groups showed marked cell growth inhibition at both 24 h and 48 h compared to the 100 or 1000 times more BSH-administrated group (Fig. 5-A). Furthermore, in the colony formation assay 2 weeks after BNCT, 8BSH-11R 1 μM and 10 μM groups had no colony formation. 800 μM and 8 mM BSH groups showed slight cell growth inhibition effects compared to the control group (Fig. 5-B, C).

Table 2
B^{10} ICP-AES results in U87 delta EGFR cell from Fig. 4-C.

^{10}B ICP-AES data *in vitro*		
Name of boron compound	^{10}B con. ($ng^{10}B/10^6$ cells) 10 μM to U87 ΔEGFR	Boron ratio (%)
BSH	15.9[a]	57.4
BSH-11R	219.4	6.0
2BSH-11R	391.4	10.0
4BSH-11R	588.8	15.1
8BSH-11R	5623.7	20.1

[a] BSH without CPPs could not penetrate cell membrane.